UNIVERSITÀ DEGLI STUDI DI NAPOLI "FEDERICO II"

DIPARTIMENTO DI FARMACIA

DOTTORATO DI RICERCA IN SCIENZA DEL FARMACO

XXV CICLO (2009-2012)

Bindarit, an anti-inflammatory agent, reduces neointimal hyperplasia in animal models of vascular injury

Relatore

Ch.mo Prof.

ARMANDO IALENTI

Coordinatore

Ch.ma Prof.ssa

MARIA VALERIA D'AURIA

Candidato

DR. MARIA VITTORIA DI LAURO

A Carlo e Ida,
che lo hanno desiderato per me,
che mi hanno sostenuta ed incoraggiata quando ero disposta a mollare.

Quanto più a fondo vi scava il dolore, tanta più gioia potete contenere.

Kahlil Gibran

CONTENTS

SUMMARY

Bindarit is an original compound with peculiar anti-inflammatory activity due to a selective inhibition of a subfamily of inflammatory chemokines, including the monocyte chemotactic proteins MCP-1/ CCL2, MCP-3/CCL7, and MCP-2/CCL8.

It is well known that chemokines have a crucial role in initiating and progressing neointima formation by controlling each step of the vascular remodelling in response to various noxious stimuli. The induction of MCP-1 not only correlates with macrophage accumulation but there is strong evidence for an important role of MCP-1 in vascular smooth muscle cell (SMC) proliferation and migration, processes that contribute substantially to neointima formation after arterial stenting and balloon angioplasty.

In this thesis, we investigated the effect of bindarit on neointima formation using three animal models of arterial injury: rat carotid artery balloon angioplasty, wire-induced carotid injury in apolipoprotein E-deficient ($apoE^{-/-}$) mice, and in stent stenosis in preclinical porcine coronary stent model.

Treatment of rats with bindarit (200 mg/kg/day) significantly reduced balloon injury-induced neointima formation by 39% at day 14 without affecting re-endothelialization and reduced the number of medial and neointimal proliferating cells at day 7 by 54 and 30%, respectively. These effects were associated with a significant reduction of MCP-1 levels both in sera and in injured carotid arteries of rats treated with bindarit. In addition, in vitro data showed that bindarit (10–300 μM) reduced rat vascular smooth muscle cell (SMC) proliferation, migration, and invasion, processes contributing to the injury-induced neointima formation in vivo.

Similar results were observed in hypercholesterolaemic $apoE^{-/-}$ mice in which bindarit administration resulted in a 42% reduction of the number of proliferating cells at day 7 after carotid injury and in a 47% inhibition of neointima formation at day 28. Analysis of the cellular composition in neointimal lesions of $apoE^{-/-}$ mice treated with bindarit showed that the relative content of macrophages and the number of SMCs were reduced by 66 and 30%, respectively, compared with the control group.

One or 2 bare metal stents (Multi-Link Vision, 3.5 mm) were deployed (1:1.2 oversize ratio) in the coronary arteries of 42 pigs (20 bindarit versus 22 controls).

Bindarit (50 mg/kg per day) was administered orally from 2 days before stenting until the time of euthanasia at 7 and 28 days. Bindarit caused a significant reduction in neointimal area (39.4%), neointimal thickness (51%), stenosis area (37%), and inflammatory score (40%,) compared with control animals, whereas there was no significant difference in the injury score between the 2 groups. Moreover, treatment with bindarit significantly reduced the number of proliferating cells (by 45%) and monocyte/macrophage content (by 55%) in stented arteries at day 7 and 28, respectively. These effects were associated with a significant ($P<0.05$) reduction of MCP-1 plasma levels at day 28. In vitro data showed that bindarit (10–300 μmol/L) reduced tumor necrosis factor-α (TNF-α, 50 ng/mL)–induced pig coronary artery smooth muscle cell proliferation and inhibited MCP-1 production.

However, the mechanisms underlying the efficacy of bindarit in controlling neointimal formation/restenosis have not been fully elucidated. Therefore, we investigated the effect of bindarit on human coronary smooth muscle cells activation, drawing attention to the phenotypic modulation process, focusing on contractile proteins expression as well as proliferation and migration.

The expression of contractile proteins was evaluated by western blot analysis on cultured human coronary smooth muscle cells stimulated with TNF-α (30 ng/mL) or fetal bovine serum (FBS, 5%). Bindarit (100-300 μM) reduced the embryonic form of smooth muscle myosin heavy chain (SMemb) while increased smooth muscle α-actin (α-SMA) and calponin in both TNF-α- and FBS-stimulated cells. These effects were associated with the inhibition of human coronary smooth muscle cell proliferation/migration and both MCP-1 and MCP-3 production.

The effect of bindarit on smooth muscle cells phenotypic switching was confirmed *in vivo* in the rat balloon angioplasty model. Bindarit (200 mg/Kg/day) significantly reduced the expression of SMemb, while increased α-SMA and calponin in rat carotid arteries subjected to endothelial denudation.

The results provided in this thesis show that bindarit given systemically significantly reduced neointimal formation in animal models of arterial injury by inhibiting SMC proliferation/migration, and macrophage infiltration; these effects correlated with a reduction in MCP-1 synthesis.

Preclinical studies demonstrated that bindarit has a safe toxicological profile and is devoid of immunosuppressive, mutagenic, and carcinogenic effects. Phase I

clinical studies demonstrated that bindarit (up to a dose of 1200 mg BID) is well tolerated and confirmed the lack of overt toxicity suggested by preclinical studies. Results of Phase II clinical studies confirmed the good tolerability profile of bindarit and demonstrated, at 600 mg BID, significant effects in kidney disease patients.

Importantly, a double-blind, randomized, placebo-controlled phase II clinical trial, with the aim of investigating the effect of bindarit in human coronary restenosis, showed that bindarit induced a significant reduction of in-stent late loss.

In conclusion, evidence of bindarit efficacy could provide clinicians with useful complementary or alternative therapeutic tools.

1. INTRODUCTION

Vascular disease constitutes a major cause of death and disability in developed countries and will soon become a health threat worldwide. This trend motivates major efforts on multiple fronts to fight cardiovascular disease, with the goals of prevention as well as improved therapy. One prerequisite for success in this quest is increased understanding of the very dynamic environment represented by the vascular wall, where several cell types interact and undergo profound phenotypic modulation in development and in diseases.

The prevalent type of CVDs in western societies *is* the coronary artery disease, in which an artery wall thickens because of the deposition of atherosclerotic plaque triggered by LDL accumulation within the artery wall.

The current procedure that allows the endovascular treatment of occlusive coronary artery disease, without the need of bypass surgery, is the percutaneous coronary intervention, commonly known as angioplasty. This procedure is executed by attaching a small balloon to a catheter. Once inflated on the stenosis, the balloon dilates the artery and improves blood flow (balloon angioplasty, Figure 1).

The most problematic complication of percutaneous coronary intervention is a well known process called restenosis, defined as the re-narrowing of the artery after initial angioplastic treatment, identifiable by a lumen diameter diagnosis of <50% at follow-up (Figure 1).

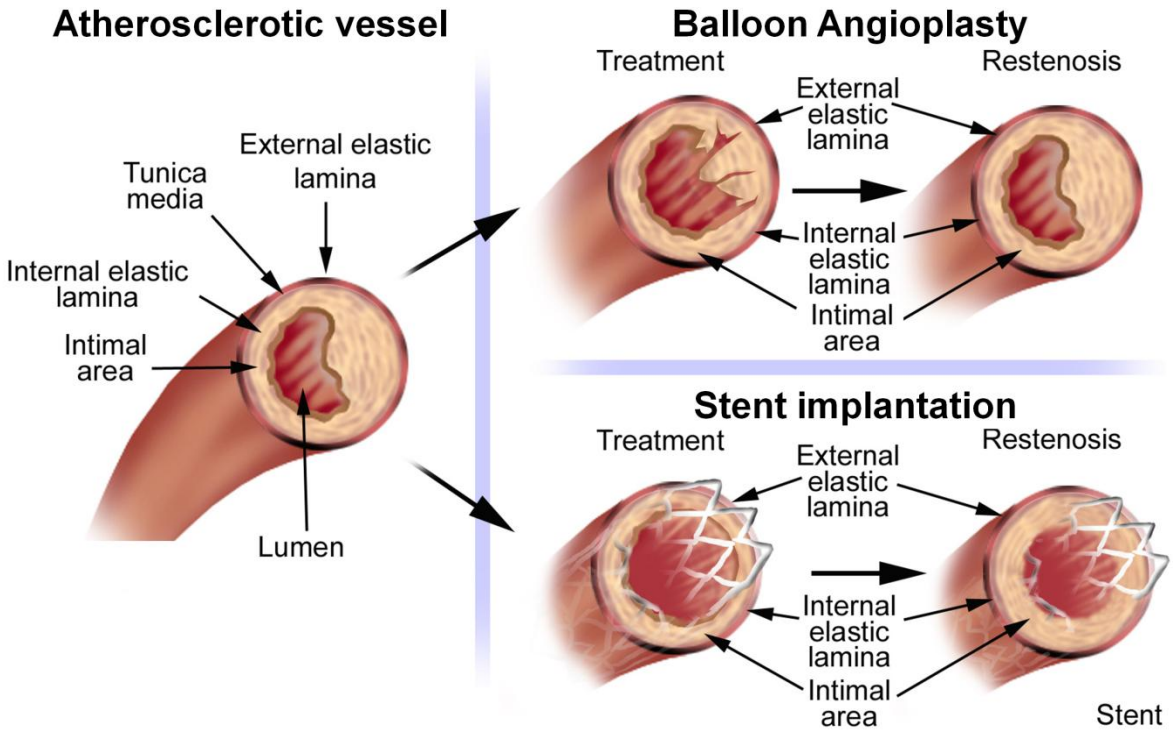

Figure 1
Mature atherosclerotic plaque before intervention (left). Restenosis after balloon angioplasty and stent implantation (right)

1.1 Restenosis

Restenosis comprises two major processes, intimal hyperplasia and vessel remodelling, and was proposed to be the arterial wall's healing response to mechanical injury. Platelet aggregation, inflammatory and immune cell infiltration, release of growth factors, vascular smooth muscle cells (SMC) proliferation, collagen deposition and extracellular matrix (ECM) remodelling were identified as the major events of this response.

However, the underlying molecular basis of restenosis remains unclear. Experimental observations support a causal correlation between inflammation and experimental restenosis (Costa MA and Simon DI 2005).

Several drugs have been used to prevent restenosis, but only a few have shown any promise in either human trials or experimental animal models. Valsartan (Peters S et al., 2001) and some statins (Walter DH et al., 2000) have been studied without any conclusive benefits. Cilostazol, an antiplatelet agent that interferes with SMCs proliferation, has shown conflicting results (Tanabe Y et al., 2001). Probucol is the first pharmacological agent showing to reduce coronary restenosis after angioplasty and the mechanism of preventing restenosis appears to be independent of its lipid-lowering effect (Tardif JC et al., 23). The

positive results obtained with probucol suggest that restenosis process is associated with oxidative stress. Reactive oxygen species are produced after angioplasty and the generation of reactive oxygen species and oxidation of lipids impairs endothelial function. Oxidative stress exerts toxic effects on SMCs which leads to the activation of inflammatory reactions (Rao GN and Berk BC, 1992). Troglitazone have also been studied with some benefits in a small human study (Takagi T et al., 2000).

The introduction of a metallic spring into the popliteal artery of an experimental animal by Charles Dotter signalled the beginning of the stent era. However, the first human stent implantation did not occur until 1986, and it was only in 1994 that the US Food and Drug Administration (FDA) approved the use of stents following two studies that conclusively proved the superiority of stents over balloon angioplasty with regards to their long term prognosis (Mitra AK and Agrawal DK, 2006). On average, stents appear to have a 10% lower rate of restenosis compared with angioplasty and the favourable results due to stent usage have been reported in several studies. Unfortunately, stents have an inherent rate of restenosis of 10-60% (Whan Lee C et al., 2008). The risk factors of restenosis include the method, lesion location (the left anterior descending artery is found to be less susceptible to restenosis), diabetes, residual stenosis, number of stents, the stent length, total occlusion and late total occlusion, and bifurcating or ostial lesions (Mitra AK and Agrawal DK., 2006). Recent technology has created a method of "coating" stents: using a coronary stent for local delivery of drugs combines scaffolding with targeted drug action. Stents coated with any of several pharmacotherapeutic agents such as heparin, hirudin, GP IIb/IIIa inhibitors, sirolimus, and paclitaxel can be used (Whan Lee C et al., 2008). The initial research and clinical trials have been concentrated on sirolimus (rapamycin), a macrolide antibiotic with immunosuppressive and anti-mitotic properties (Whan Lee C et al., 2008). Prospective, randomized clinical trials have shown that in-stent restenosis is reduced by the use of drug-eluting stents, as compared with bare-metal stents (Lagerqvist B et al., 2007). On the basis of prospective trials involving approximately 4500 patients, the FDA approved the use of drug-eluting stents (Lagerqvist B et al., 2007). With the increased usage of the stents, there are reports of problems, such as late stent malapposition, subacute and late thromboses and aneurysm formations due to the toxicity associated with this method of treatment. In addition, the long term effects of stents are still unknown. Recent reports suggest that drug-eluting stents may increase the risk of stent thrombosis relative to bare-metal stents (Yan BP et al., 2008).

1.2 Pathogenesis of restenosis

Restenosis is a hyperplastic, pathologic reaction involving SMCs migration and proliferation, ECM formation and remodelling of the arterial wall leading finally to reocclusion of the enlarged artery. Similarly to early, fibrous atheromas, human restenotic lesions consist mainly of fibrocellular tissue (Virmani R et al., 1994).

Within minutes following balloon deflation, the artery undergoes elastic recoil due to contraction of the elastic fibers of the inner and external lamina, causing up to a 40% lumen loss. A thrombotic response triggered by endothelial denudation, and medial dissection due to the mechanical injury of the angioplasty procedure, lead to platelet adherence and aggregation on the exposed sub-endothelial surface. Neointimal formation is a complicated process involving the recruitment of inflammatory cells to the site of injury, the migration of SMCs from the media to the intima, and the proliferation of these cells. Growth factors and cytokines are the major stimuli for proliferation of SMCs after the injury (Serruys PW et al., 1988). The earliest step in the process of in-stent restenosis, before SMCs proliferation, is platelet deposition and aggregation (Chandrasekar B et al., 2000). Platelets release multiple growth and migratory-promoting factors in addition to those released from injured vascular cells and surrounding extracellular matrix such as thrombin, platelet-derived growth factor (PDGF), interleukin (IL)-1, insulin-like growth factor-1 (IGF-1), fibroblast growth factor-2 (FGF-2), vascular endothelial cell growth factor (VEGF), and others (Topol EJ and Serruys PW, 1998; Lincoff AM et al., 1994). This complex interplay of growth factors then regulate SMCs migration and proliferation through cell surface receptors and intracellular signalling molecules inducing early response genes necessary for cells to leave their quiescent state and enter the cell cycle (Sherr CJ and Roberts JM, 1999). The dynamic process of SMCs migration involves changes in matrix synthesis such as degradation and organization (Galis ZS and Khatri JJ, 2002). Matrix metalloproteinases, effectors of extracellular matrix degradation are upregulated after injury and the degradation of the extracellular matrix allows SMCs to migrate to the intima (Galis ZS and Khatri JJ, 2002).

Restenosis after balloon angioplasty seems to be determined primarily by the direction and magnitude of vessel wall remodeling. In contrast, the major limitation of stent implantation is the initiation of neointimal tissue proliferation within and adjacent to the stent (Indolfi C. et al., 1999).

1.2.1 Vascular smooth muscle cell activation

SMC activation is a prominent mechanism of the intimal hyperplasia at the base of the restenosis. Normally, vascular SMCs the media reside in a quiescent, differentiated state, and express a unique repertoire of contractile proteins to keep vascular tone by contraction or relaxation thus being referred to contractile phenotype. However, SMCs maintain considerable plasticity (Owens GK et al., 2004). After disruption of the normal steady state by vascular injury or disease, SMCs undergo a process often referred to as phenotypic modulation/switching characterized by dramatic increases in the rates of proliferation, migration, and synthesis of ECM proteins, growth factors and inflammatory mediators, along with decreased expression of SMC-specific/-selective marker genes such as smooth muscle α-actin (α-SMA), smooth muscle-myosin heavy chain (SM-MHC), SM22α, h1-calponin, smoothelin, caldesmon, and telokin (Owens GK et al., 2004).

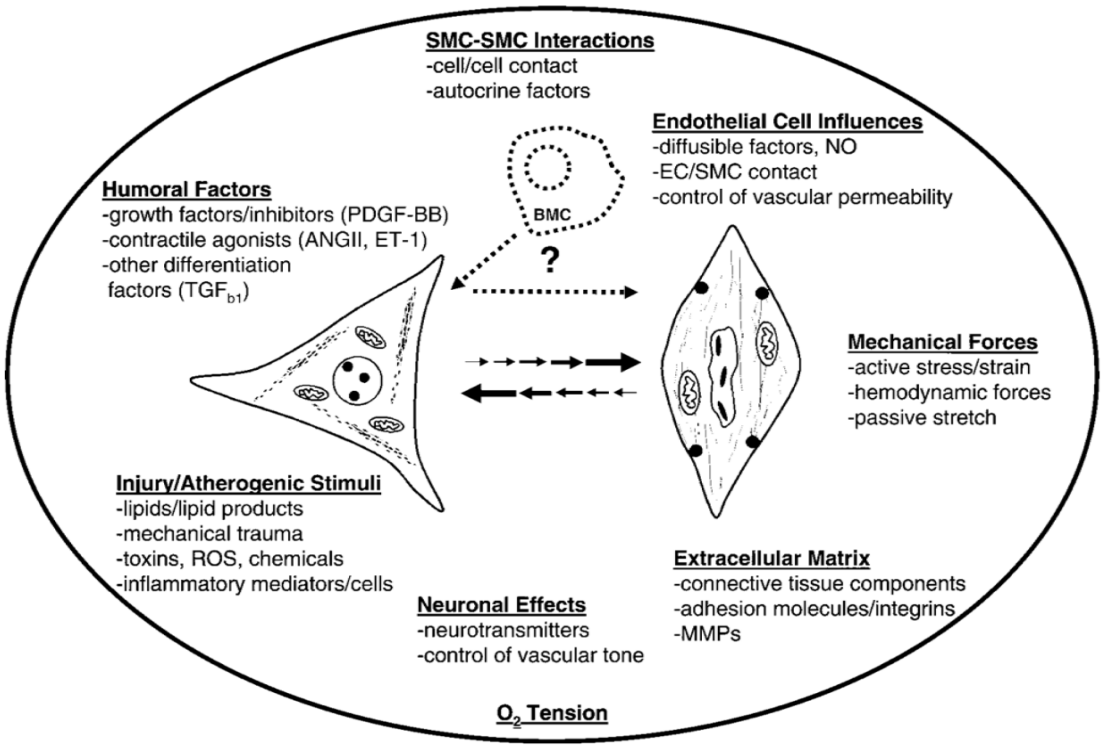

Figure 2
The differentiation state of SMCs is highly plastic and dependent on integration of multiple local environmental cues (Figure adapted from Owens GK et al., 2004).

Early markers of SMC activation, such as expression of nuclear oncogenes are detectable as soon as 30 minutes after injury (Bauters C et al., 1992) and/or several hours after angioplasty, is associated with the early G_1 events preceding DNA synthesis in SMCs.

Although it is still unclear what actually triggers the process of phenotypic modulation *in vivo*, injurious stimuli are known to alter the environment of the vascular wall by affecting endothelial function and inducing platelet adhesion and activation, migration of immune cells and changes in the ECM. These environmental changes subsequently induce the production of growth factors and cytokines by SMCs, which in turn activate autocrine/paracrine pathways leading to further phenotypic modulation. For example, in atherogenesis, PDGF produced by SMCs and other cell types, was shown to down regulate SMC differentiation markers such as α-SMA and SM-MHC (Owens GK et al., 2004); matrix degrading proteases produced by macrophages may contribute to the degradation of the basement membrane (Galis ZS et al., 1994), and in restenosis, proteases may also derive from the injured SMCs present in the lesion (Yoshida T and Owens GK, 2005). This activation renders the SMCs responsive to chemoattractants and mitogens resulting in subsequent migration and proliferation, both processes contributing to neointimal hyperplasia.

1.2.2 Immune/Inflammatory response

For several decades immune modulation of neointimal formation after vascular injury has been investigated but the complexities involved continue to obscure a clear understanding of this process. However, both antigen-specific and nonspecific immune responses could occur during restenosis.

The major detrimental in innate immune responses associated to vascular injury is the macrophage infiltration. De-endothelialisation, provoked by balloon dilatation of the arterial wall, in fact, allows to a layer of platelets and fibrin to deposit at the injured site (Toutouzas K et al., 2004). An interaction between platelets and leukocytes, that involves the platelet P-selectin and the β2 integrin molecule Mac-1 (CD11b/CD18), promotes a process of leukocyte recruitment and infiltration, which is critical to the inflammatory response (Welt FGP and Rogers C, 2002). Analysis of human arterial segments also suggests a critical role of inflammation during in-stent restenosis. In the initial phase, post-stent implantation, the mural thrombus formation is followed by activation and invasion of SMCs, T-lymphocytes and macrophages. After this early neointimal formation, extracellular matrix increases; growth factors, cytokines and chemokines are released from leukocytes, SMCs and

endothelial cells, thus enhancing the migration of leukocytes across the platelet-fibrin layer into the tissue and inducing fibroblast proliferation and transformation to myofibroblasts (Toutouzas K et al., 2004). Many chemokines such as interleukin (IL)-8, participate in the recruitment of monocytes, leukocytes and neutrophils to areas of vascular injury (Welt FGP and Rogers C, 2002). Others, like monocyte chemoattractant protein (MCP)-1, are involved in the recruitment of monocytes, basophils and T cells (Welt FGP and Rogers C, 2002), as well as activation of SMCs (Charo IF and Taubman MB, 2004). Lately a key player in fundamental mechanisms, regulating the development of restenosis, as inflammation and proliferation, is the ubiquitin–proteasome system of intracellular protein degradation. Proteasome, in fact, is required for the activation of the transcription factor "*nuclear factor-κB*" (NF-κB) by degrading its inhibitory IκB protein. Once activated, NF-κB induces the transcription of a large number of genes codifying for cytokines and chemokines involved in inflammatory and immune responces (Hayden MS and Ghosh S, 2008) as well as a variety of genes related to cell differentiation, apoptosis, and proliferation (Karin M, 2006). Cell apoptosis or necrosis, occurring during injury, may trigger the release of intracellular material, including uric acid and heat-shock proteins that can further enhance the immune activation (Dimayuga PC et al., 2010).

The adaptive immune response appears to be more complex. Prior studies suggest that B lymphocytes inhibit neointimal formation (Dimayuga PC et al., 2005), likely through the production of immunoglobulin. Similarly, experiments based on using T-cell depletion, T-cell deficiency, or T-cell transfer indicate the inhibitory role of these cells in arterial injury (Hansson GK et al., 1991; Remskar M. et al., 2001; Dimayuga PC et al., 2005). It has been observed that T lymphocytes also regulate the repair processes of the vasculature to injury by inhibiting SMC proliferation (Hansson GK et al., 1991). Although these data suggest a protective role of immune cell activation in response to arterial injury, it has been proposed that dendritic cells, also present in neointimal lesions, may have the capacity to induce autoimmune responses in T cells (Han JW et al., 2008) exacerbating the inflammatory response after vascular injury (Fig. 3). Because the role of T lymphocyte is still unknown, few studies have been conducted to investigate the effect of drug eluting stent in spite of the use of antiproliferative/immunesuppressive drugs. One study showed a significant reduction in T lymphocyte infiltration 8 months after DES implantation; another study showed that sirolimus DES increased CD8+ central memory T cells (Dimayuga PC et al., 2010).

It stands to reason that the role of both innate and adaptive immunity in restenosis remains still unclear, thus further studies are needed to obtain a more comprehensive view of

this growth regulatory network, also to investigate the benefit of current therapy, especially DES.

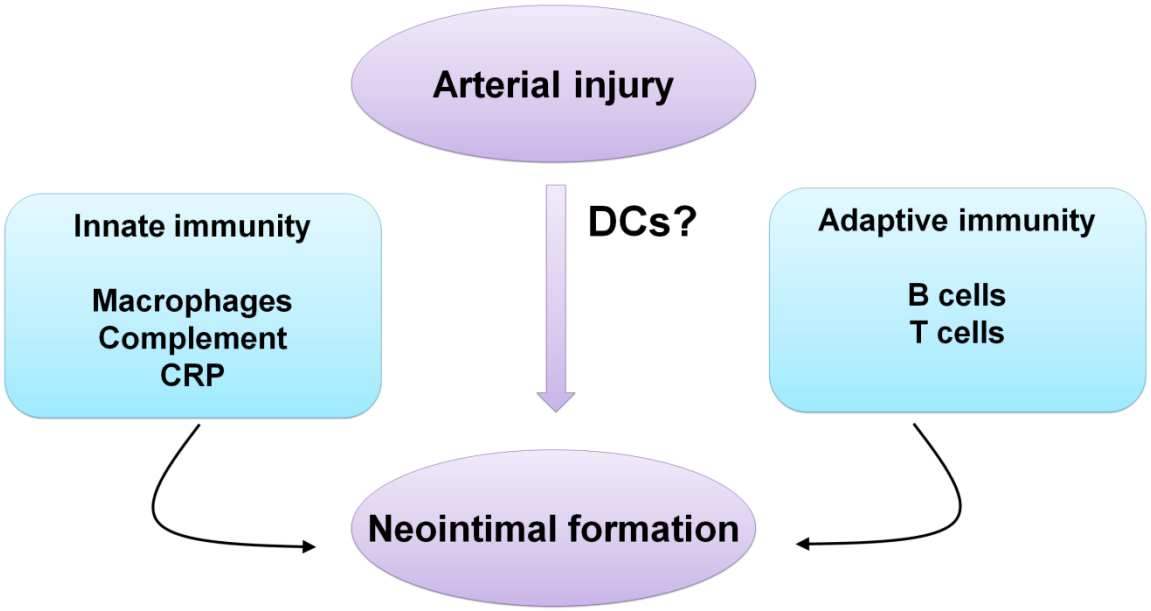

Figure 3
Immune response to arterial Injury

1.3 Chemokines as therapeutic targets in vascular pathology

In humans, the chemokines (chemotactic cytokines) system includes 42 ligands grouped in four subfamilies (C, CC, CXC, and CX3C) on the basis of the number and position of N-terminal-conserved cysteine residues (Figure 4).

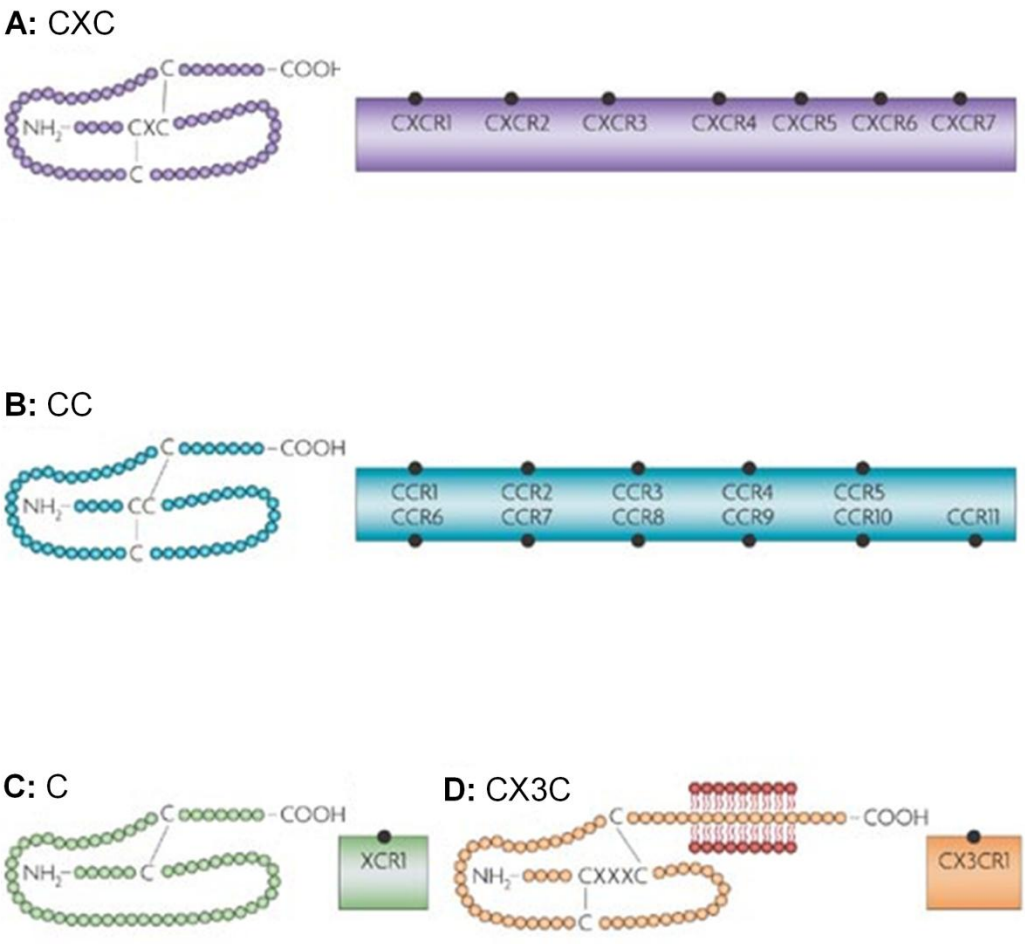

Figure 4
Classification of the four families of chemokines and their respective receptors (Figure adapted from Rostène et al., 2007)

"CXC" chemokines represent one major chemokine family and are characterized by the presence of two cysteines, nearest the N-termini, separated by a single amino acid. The prototypical member of CXC chemokines is IL-8. The other major chemokine family is called "CC" because the two cysteines are adjacent. CC chemokines are RANTES, macrophage inflammatory protein-1α (MIP-1α) and MIP-1β and the monocyte chemotactic protein (MCP) subfamily including MCP-1, MCP-2, MCP-3, MCP-4 and MCP-5. The third family of chemokines is denoted "C" because of the lone cysteine in the N-terminal domain. Two chemokines have been described for this group and are called XCL1 (lymphotactin-α) and XCL2 (lymphotactin-ß). The last family, the "CX3C" family, has only one known member, fractalkine (FK or CX3CL1) that consists of a soluble chemokine domain fused to a mucin-like stalk and a transmembrane domain.

Chemokines exert their cellular effects by activating seven transmembrane–domain G-protein–coupled receptors. Different cell types are characterized by different complements of chemokine receptors; this determines whether cells respond to a particular chemokine set. Chemokine binding to receptor triggers an intracellular signal transduction cascade that activates phosphatidylinositol-3 kinase, increases levels of inositol trisphosphate and intracellular calcium, activates Rho and mitogen-activated protein kinases. These events cause cell responses, including actin re-arrangement, shape change and chemotaxis. Chemokine receptors are divided into different families, CXC chemokine receptors, CC chemokine receptors, XC chemokine receptors and CX3C chemokine receptors that correspond to the four distinct families of chemokines they bind (Figure 4).

Chemokines and their receptors have a crucial role in initiating and progressing neointimal formation by controlling each step of the vascular remodelling in response to various noxious stimuli (Schober A, 2008). Chemokines are produced by the major cells of the arterial wall, such as endothelial cells, SMCs, adventitial fibroblasts, leukocytes, as well as the circulation. They direct the leukocyte trafficking and activate the SMCs during vascular pathology (Schober A, 2008). SMCs, in fact, respond to a number of chemokines involved in cell proliferation or intracellular calcium mobilization resulting in induction of tissue factor (Charo IF and Taubman MB, 2004), a key factor in the pathogenesis of acute coronary syndromes. It is well known that MCP-1 direct the monocyte homing (Schober A, 2008) as well as SMC proliferation and migration (Selzman CH et al., 2002; Massberg S et al., 2003). RANTES induces the leukocyte recruitment through different chemokine receptors (Schober A, 2008) and fractalkine induces both inflammation and SMC proliferation during neointimal formation (Schober A, 2008). Eotaxin induces migration of cultured SMCs (Kodali RB et al., 2004).

The importance of chemokines in vascular diseases has sparked intense interest in developing broad-based inhibitors of chemokine activity as therapeutic agents. Several drugs, already in use as a treatment of vascular pathology or its risk factors, are able to modify the chemokine expression. For instance, HMG-CoA reductase inhibitors have been demonstrated to reduce, *in vitro* and *in vivo*, the expression of several markers of vascular inflammation, including chemokines (Apostolakis S et al., 2006). Similar findings have been demonstrated for angiotensin converting enzyme (ACE) inhibitors, angiotensin II receptor blockade and glitazones (Apostolakis S et al., 2006). Thus, some widely used anti-atherogenic drugs could mediate their beneficial actions partially through inhibition of certain chemokine pathways.

Directly blocking chemokine activation is now the goal of prevention as well as therapy of vascular disease and several preclinical studies are ongoing in this sense. It has been demonstrated that intravenous infusion of the myxoma virus M-T7, that inhibits CC and other chemokines, markedly reduced intimal hyperplasia in a rabbit model of arterial injury (Charo IF and Taubman MB, 2004). The chemokine antagonist MET-RANTES reduced neointimal formation in apolipoprotein E-deficient ($apoE^{-/-}$) mice as well as atherosclerotic plaque formation in $LDLR^{-/-}$ mice (Charo IF and Taubman MB, 2004).

Since initiation and development of atherosclerosis and intimal hyperplasia after vascular injury are regulated by MCP-1 (Boring L et al., 1998; Egashira K et al., 2002), MCP-1/CCR2 pathway is recently receiving increasing attention. It has been observed that eliminating the MCP-1 gene or blocking MCP-1 signalling decreases neointimal hyperplasia in several animal models of vascular injury (Furukawa Y et al., 1999; Egashira K et al., 2007). Catheter-based adenovirus-mediated anti-monocyte chemoattractant gene therapy attenuates in-stent neointimal formation in monkeys (Nakano K et al., 2007). Up to now the possibility to use an oral inhibitor of MCP-1 pathway, has not yet been investigated. In this regard, an original indazolic compound, called bindarit, has been identified. Bindarit inhibits MCP-1 synthesis and its ability in reducing neointimal formation has been subject of this thesis.

In the context of MCP-1/CCR2 pathway activation during vascular injury, it is interesting to note that $CCR2^{-/-}$ mice have a ≈60% decrease in intimal hyperplasia and medial DNA synthesis in response to femoral arterial injury while $MCP\text{-}1^{-/-}$ mice show a ≈30% reduction in intimal hyperplasia, which is not associated with diminished medial DNA synthesis (Charo IF and Taubman MB, 2004). These data suggest that MCP-1 and CCR2 deficiencies have distinct and separate effects on arterial injury; therefore, it is possible that the results obtained with $CCR2^{-/-}$ mice may not be solely mediated by MCP-1 but also by other chemokines acting on the same receptor. It is known that CCR2 is shared with MCP-3 and that this chemokine acts through interaction with not only CCR2 but also CCR1 and CCR3, all expressed on vascular SMCs. The role of MCP-3 in vascular pathology is not well known.

Although in the past few years we have witnessed a rapid increase in our understanding of the role of chemokines and their receptors in cardiovascular pathologies, all investigators agree on the fact that the precise mechanism of the chemokine pathways involved in the response of the arterial wall to vascular injury is not fully elucidated. Much more information is needed before chemokine-based therapies can be applied in clinical practice.

1.4 Bindarit

Bindarit, or 2-methyl-2-{[1-phenylmethyl)-1H-indazol-3-y1]methoxy} propanoic acid is an original indazolic derivative (Fig. 5), synthesized by Angelini (Angelini Research Center—ACRAF, Italy), devoid of any immunosuppressive effects and with no activity on arachidonic acid metabolism that was shown to have anti-inflammatory activity in a number of experimental animal models of both acute and chronic inflammation. These pharmacological activities have been associated with its ability to interfere with monocyte recruitment in inflamed tissues, which has been ascribed to a selective inhibitory effect on the monocyte chemotactic protein (MCP) subfamily of CC inflammatory chemokines, including MCP-1/CCL2, MCP-3/ CCL7, and MCP-2/CCL8 (Bhatia M et al., 2005).

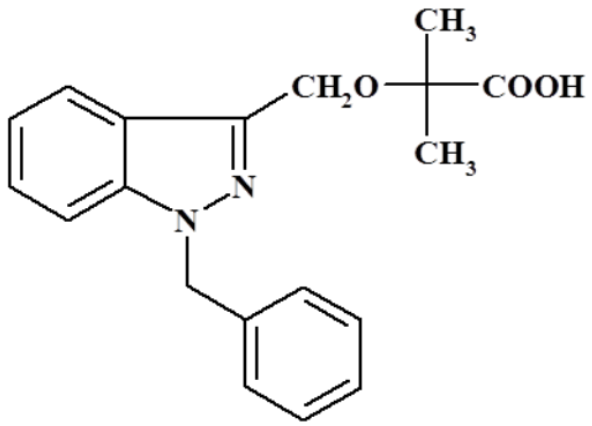

Figure 5
2-methyl-2-{[1-phenylmethyl)-1H-indazol-3-y1]methoxy} propanoic acid (bindarit)

Zoja C. et al. (1998) demonstrated that bindarit retards renal disease and prolongs survival in NZB/W mice that have a spontaneous autoimmune disease reminiscent of human systemic lupus erythematosus. In fact, bindarit delayed the onset of proteinuria and significantly protected from renal function impairment. Appearance of anti-DNA antibodies was retarded and survival significantly prolonged by bindarit. Bindarit significantly limited glomerular hypercellularity, interstitial inflammation and tubular damage. Renal expression of monocyte chemoattractant protein (MCP-1) mRNA (Northern blot) markedly increased during the progression of nephritis in association with mononuclear cell infiltration. Bindarit completely prevented MCP-1 up-regulation. In another series of experiments, bindarit when

started at 4.5 months of age in NZB/W mice improved survival in respect to untreated mice in a dose-dependent manner.

Furthermore, Guglielmotti A et al. (2002) demonstrated that bindarit ameliorates rats arthritis induced by Freund's complete adjuvant injection. The course of arthritis was monitored by sequential paw volume measurement and by radiologic and histologic evaluations. Bindarit possessed therapeutic activity resulting in a significant inhibition of paw inflammation. Evidence for a disease-modifying activity was also indicated by amelioration of radiologic alterations and by histological evaluation of joints. Additional evidence for beneficial effects in osseous inflammation was provided by an in vitro assay in which bindarit inhibited the release of MCP-1 from IL-1 stimulated human osteoblast cells. Moreover, in a murine model of LPS-induced cytokine production bindarit reduced MCP-1 and tumor necrosis factor (TNF)-α increase without affecting IL-1 and IL-6 levels.

In a model of acute pancreatitis induced by caerulein hyperstimulation, Bhatia M et al. (2005) demonstrated that prophylactic as well as therapeutic treatment with bindarit significantly reduced MCP-1 levels in the pancreas. Also, this treatment significantly protected mice against acute pancreatitis as evident by attenuated hyperamylasemia neutrophil sequestration in the pancreas (pancreatic MPO activity), and pancreatic acinar cell injury/necrosis on histological examination of pancreas sections.

In human intestinal epithelial cells (HT-29) bindarit concentration-dependently and selectively inhibited MCP-1 secretion (as well as mRNA expression) primed by TNF-α/IFN-γ. These effects were associated with significant inhibition of MCP-1 and myeloperoxidase (MPO) activity in colon extracts. Bindarit exhibits a potent bioactivity in reducing leukocyte infiltration, down-regulating MCP-1 synthesis, and preventing the development of severe colitis in a mice model of TNBS-induced colitis suggesting a potential use of MCP-1 synthesis blockers in intestinal inflammation in humans (Bathia M et al., 2008).

Monocyte chemoattractant proteins mediate myocardial microvascular dysfunction in swine renovascular hypertension (HTN) that is associated with inflammation as well as impaired cardiac microcirculatory function and structure. Lin J et al. (2009), tested the hypothesis that MCPs regulate cardiac microvascular function and structure in swine renovascular HTN model. Pigs were studied after 10 weeks of normal, renovascular HTN, or renovascular HTN+ bindarit as MCPs inhibitor. Left ventricular (LV) function, myocardial microvascular permeability, and fractional vascular volume were assessed by fast computed tomography before and after adenosine infusion. Myocardial fibrosis, inflammation, and microvascular remodeling were determined *ex-vivo*. HTN upregulated

endothelin-1 expression, myocardial inflammation and microvascular wall thickening, which were inhibited by bindarit. MCPs partly mediate myocardial inflammation, fibrosis, vascular remodeling, and impaired vascular integrity induced by hypertension. Inhibition of MCPs could potentially be a therapeutic target in hypertensive cardiomyopathy.

The molecular mechanisms responsible for the inhibitory effect of bindarit on monocyte recruitment are still unclear. Recently, Mora E et al. (2012) demonstrated in both a mouse leukaemic monocyte-macrophage cell line and bone marrow-derived macrophages, that the inhibitory effect of bindarit is mediated by the downregulation of the classical NF-kB pathway, involving a reduction of IkBα and p65 phosphorylation, a reduced activation of NFkB dimers and a subsequently reduced nuclear translocation and DNA binding. Bindarit showed a specific inhibitory effect on the p65 and p65/p50 induced MCP-1 promoter activation, with no effect on other tested activated promoters (IL-12b/p40, IL-6 and IL-8/KC). The Authors concluded that bindarit acts on a specific subpopulation of NF-kB isoforms and selects its targets within the whole NF-kB inflammatory pathway.

Interestingly, phase II clinical trials have shown that bindarit is well tolerated and significantly reduced urinary MCP-1 and albumin excretion in kidney disease (Perico N et al., 2008; Guglielmotti A et al., 2009).

1.5 Specific aims

We evaluated the effect of bindarit on neointimal formation in animal models of vascular injury such as rat carotid artery balloon angioplasty, wire-induced carotid injury in apolipoprotein E-deficient (apoE$^{-/-}$) mice, and in-stent stenosis in the preclinical porcine coronary stent model. In addition, we also investigated the effect of bindarit on human coronary vascular SMC activation, drawing attention to the phenotypic modulation process, focusing on contractile proteins expression as well as proliferation and migration.

The results provided in this thesis strongly support the beneficial effects of bindarit on the inflammatory/proliferative processes leading to neointima formation.

2. METHODS

2.1 In vitro experiments

2.1.1 Cell culture

Primary rat or murine vascular SMCs were isolated from the thoracic aorta of male Wistar rats or female apoE$^{-/-}$ mice as previously described (Parenti A et al., 2004). Porcine vascular SMCs were isolated from coronary arteries of male pigs as previously described (Work LM et al., 2001).

Cells were grown in Dulbecco's modified Eagle medium (DMEM; Cambrex Bio Science) supplemented with L-glutamine, 10% fetal bovine serum (FBS, Lonza), 100 U/mL penicillin, and 100 μg/mL streptomycin, in a humidified incubator at 37 °C in 5% CO2, and used between passages 3 to 6 for all experiments. Before initiation of assays, to achieve cell quiescence, SMCs in exponential growth were switched into DMEM supplemented with 1% FBS for 48 hours.

Human Coronary Artery Smooth Muscle Cells (CASMCs) were purchased from Lonza (lot numb: 6F4008 and 16737) (Maddaluno et al., 2012), grown in Smooth Muscle Basal Medium (SmBM; Lonza) supplemented with 0.5 mg/mL hEGF, 5 mg/mL insulin, 1 mg/mL hFGF, 50 mg/mL gentamicin/amphotericin-B, 5% fetal bovine serum (FBS, Lonza), in a humidified incubator at 37 °C in 5% CO2 and used between passages 3 to 8 for all experiments. Before initiation of the assays, CASMCs in exponential growth were switched into SmBM supplemented with 0.1% FBS in the absence of growth factors for 48 hours.

2.1.2 Proliferation assay

Cell proliferation was evaluated using the 3-(4,5-dimethylthiazol-2-yl)-2,5-diphenyltetrazolium (MTT) assay.

SMCs were plated on 48 multi-well plastic culture plates at the density of $1.5x10^4$ cells/well. After the induction of quiescence, rat or murine SMCs were stimulated with platelet derived growth factor-BB (PDGF-BB,10 ng/mL, R&D Systems) for 48 hours, porcine SMCs were stimulated with human tumor necrosis factor-α (TNF-α, 50 ng/mL, R&D Systems) for 72 hours, and CASMCs were stimulated with TNF-α (30 ng/mL, Provitro) or FBS (5%) for 48 hours, in the presence or absence of bindarit (10-300 μM).

0.5 mg/ml of MTT in Phosphate Buffered Saline (PBS) were added and, after 3 hours, a solution containing 50% N,N'-dirnethylformamide and 20% SDS (pH 4.8) was used for the solubilisation of the formazan dye. Absorbance values at 570 nm were determined the next

day with an Enzyme-linked immunosorbent assay (ELISA) assay reader (Bio-Rad), using 630 nm as the reference wavelength.

CASMC proliferation was also evaluated as cell duplication by directly counting the cell number. Briefly, $1x10^4$ cells were seeded onto 24-well plastic culture plates and allowed to adhere overnight. After the induction of quiescence, the cells were stimulated with TNF-α (30 ng/mL) or FBS (5%) in presence or absence of bindarit (10–300 μM). After 72 hours, medium was removed, cells were fixed with methanol and stained with 4',6- diamidino-2-phenylindole (DAPI). Proliferation was evaluated as cell duplication by counting the number of cells in 8 random fields of each well at x100 magnification.

2.1.3 Chemotactic Migration and Invasion

Vascular SMC migration was evaluated using a modified Boyden chamber (Corning 24 mm Transwell with 8.0 μm pore polycarbonate membrane insert) coated with rat-tail collagen I (Sigma-Aldrich). Biocoat Matrigel invasion chambers (with 8.0 μm pore) were used according to the manufacturer's instructions for invasion studies (Becton–Dickinson). Briefly, starved SMCs were trypsinized and pre-treated or not with bindarit (10-300 μM) for 2 hours.

Rat aortic SMCs were plated in the upper chamber at the density of $5x10^5$ cells in 150 μL of DMEM 1%, whereas CASMCs were plated in the upper chamber at the density of $3x10^4$ cells in 500 μL of SMBM 0.1%, with or without bindarit.

The lower chamber was filled with 600 μL of DMEM 1% or SMBM 0.1% in the absence (untreated cells) or presence of PDGF-BB 10 ng/mL or TNF-α (30 ng/mL) respectively.

Rat SMC migration and invasion were evaluated respectively after 6 hours or 48 hours and quantified by counting the number of cells in eight randomly chosen fields per insert.

CASMC migration and invasion were evaluated after 24 hours. Migrated cells were fixed and stained with haematoxylin. Cell chemotaxis was quantified by counting the number of cells (magnification x200) per insert.

2.1.4 Enzyme-Linked Immunosorbent Assay (ELISA) on SMCs supernatans

SMCs were plated as above. After the induction of quiescence, rat SMCs were stimulated with 10 ng/mL PDGF-BB (6-48 hours), porcine SMCs were stimulated with 50 ng/mL TNF-α (12-72 hours), CASMCs were stimulated with 30 ng/mL TNF-α (6-48 hours), in the presence or absence of bindarit (10-300 μM).

Media were collected and centrifuged at 2000*g* for 15 minutes at 4 °C, and supernatants were immediately frozen at -80 °C until use. Supernatants from rat and porcine SMCs were used for MCP-1 measurement by ELISA according to the manufacturer's instructions (OptEIATM, Biosciences, and Pig CCL-2 ELISA kit, Bethyl Laboratories, Montgomery, TX). Supernatants from CASMCs were used for MCP-1 (OptEIA, BD) or MCP-3 (Quantikine Human CCL7/ MCP-3 Immunoassay, R&D Systems) measurement by ELISA.

2.1.5 Evaluation of CASMC Morphological Changes

CASMCs were used after the induction of quiescence in 48-well plastic culture plates at the density of $1x10^4$ cells/well. Cells were stimulated with FBS (5%) in presence or absence of bindarit (300 μM). After 48 hours cells were photographed at a magnification of ×200 and the images were stored in the image analysis system (LAS, Leica).

2.1.6 Measurement of MMP-2 and MMP-8 Activity by Gelatin Zymography

CASMCs were cultured in 96 multi-well culture plates in 10% FBS medium until 90% confluence. After the induction of quiescence, cells were stimulated with TNF-α (30 ng/mL) in the presence or absence of bindarit (300 μM). After 24 hours the media were collected, clarified by centrifugation and subjected to electrophoresis in 8% SDS-PAGE containing 1 mg/mL gelatin. After electrophoresis the gels were re-natured by washing with 2.5% Triton X-100, to remove SDS, and by incubation for 24 hours at 37 °C in 50 mM Tris buffer containing 200 mM NaCl and 20 mM CaCl2, pH 7.4. The gels were stained with 0.5% Coomassie brilliant blue R-250 (Sigma) in 10% acetic acid and 45% methanol and destained with 10% acetic acid and 45% methanol. Bands of gelatinase activity appeared as transparent areas against a blue background. Gelatinase activity was then evaluated by quantitative densitometry.

2.1.7 Total Cellular Extracts

CASMCs were cultured in 24 multi-well plates until 90% confluence. After the induction of quiescence, cells were stimulated with TNF-α (30 ng/mL) or FBS (5%) in presence or absence of bindarit (100-300 μM). After 48 hours cells were washed two times with ice cold PBS and 30 μL/well of lysis buffer (50 mM Tris-HCl, 1% Triton, 1 mM Na3VO4, 1 mM EDTA, 0.2 mM PMSF, 25 μg/mL Leupeptin, 10 μg/mL Aprotinin, 10 mM NaF, 150 mM NaCl, 10 mM β-glycerophosphate, 5 mM pyrophosphate, H2O) were added. Protein concentration was determined by the Bio-Rad protein assay kit (Bio-Rad).

2.1.8 Western blot Analysis on CASMCs

CASMCs lysates (20 μg) were separated by Sodium Dodecyl Sulphate - PolyAcrylamide Gel Electrophoresis (SDS-PAGE), transferred onto nitrocellulose membranes (Millipore) and probed with a primary antibody against human α-SMA (1:5000, Sigma- Aldrich), calponin (1:5000, Sigma-Aldrich) or MYH9/10 (SMemb, 1:2000, Santa Cruz). The membranes were washed three times with 0.5% Triton in PBS and incubated with anti-mouse immunoglobulins coupled to peroxidase (1:1000; DAKO). The immunocomplexes were visualised by the enhanced chemiluminescence (ECL) method, results were analyzed by ImageJ densitometry software and normalized to β-actin.

2.2. In vivo experiments

2.2.1 Animals

Male Wistar rats (250 g, Harlan Laboratories) and 8 weeks-old female apoE$^{-/-}$ mice (Charles River) on a 12-hour light/dark cycle with free access to food and water, were maintained at the Department of Experimental Pharmacology, University of Naples Federico II. All procedures were performed according to Italian ministerial authorization (DL 116/92) and European regulations on the protection of animals used for experimental and other scientific purposes.

Male large-white/Landrace healthy pigs (20–24 kg, 10 weeks old, SAC Commercial Ltd, Edinburgh, United Kingdom) on a 12-hour light/dark cycle, with free access to water and twice-daily food, were maintained at the Biological Procedures Unit, University of Strathclyde. All procedures were performed in accordance with local ethical and UK Home Office regulations.

2.2.2 Bindarit Administration

Bindarit, 2-methyl-2-[[1-(phenylmethyl)-1H-indazol-3-yl]methoxy] propanoic acid (MW 324.38), was synthesized by Angelini (Angelini Research Center-ACRAF, Italy). Pharmacokinetic studies in rodents show that bindarit is well absorbed when administered by oral route, and it has a mean half-life of ~9 h and, at dose regimen used in this study, reaches plasma levels in the range of 150-450 μM (Product data sheet, Angelini Research Center).

Rats were treated with bindarit, suspended in 0.5% methylcellulose aqueous solution, at the dose of 100 mg/kg given orally, by gastric gavage, twice a day from 2 days before angioplasty up to 14 days after, whereas apoE$^{-/-}$ mice were dosed (100 mg/kg/os/bid) from

7 days before endothelial denudation up to 28 days after. In each experiment, control animals received an equal volume of methylcellulose (0.5 mL/100 g in rats; 0.1 mL/10 g in mice).

Pigs were treated with bindarit at the dose of 25 mg/kg given orally twice a day (12-hour interval). Dosing started 2 days before stenting and continued daily for the 7 or 28 day follow-up period. The bindarit powder was mixed with yogurt and squirted into the pigs' mouths. Control animals received vehicle alone (yogurt containing no bindarit).

The dose regimen of bindarit was chosen based on earlier results from a swine renovascular hypertension model (Lin J et al., 2009; Zhu XY et al., 2009) and pharmacokinetic studies in male Göttingen minipigs (10–12 kg, Harlan) showing that bindarit is well absorbed when administered by the oral route. Single-dose oral administration of 25 mg/kg resulted in a C_{max} level of 50 μg/mL (corresponding to 154 μmol/L), T_{max} 2 hours, and t½ ≈ 10 hours (Product Data Sheet, Angelini Research Center), corresponding to concentrations able to inhibit MCP-1 production and inflammation (Lin J et al., 2009; Zhu XY et al., 2009; Zoja C et al., 1998).

2.2.3 Surgical procedures

2.2.3.1 Rat carotid ballon angioplasty

Rats were anaesthetized with an intraperitoneal injection of ketamine (100 mg/kg) (Gellini International) and xylazine (5 mg/kg) (Sigma). Endothelial denudation of the left carotid artery was performed with a balloon embolectomy catheter (2 F, Fogarty, Edwards Lifesciences) according to the procedure well validated in our laboratories (Maffia P et al., 2006)

Some animals were subjected to anaesthesia and surgical procedure without balloon injury (sham-operated group). Rats were euthanized 1, 7, 14, and 28 days after angioplasty. Blood and carotid arteries were collected and processed as described below.

2.2.3.2 Wire-induced carotid injury in apoE$^{-/-}$ mice

ApoE$^{-/-}$ mice were fed an atherogenic diet (21% fat, 0.15% cholesterol, 19.5% casein, wt/wt; TD88137, Mucedola) from 1 week before until 4 weeks after carotid injury performed as described previously (Jeremy JY et al., 2010), with minor modification. Briefly, mice were anaesthetized as described above, and endothelial injury of the left common carotid artery was performed with a 0.35 mm diameter flexible nylon wire introduced through the left external carotid artery and advanced to the aortic arch. The

endothelium was damaged by passing the wire through the lumen of the artery three times. ApoE$^{-/-}$ mice were euthanized 7 and 28 days after wire injury. Blood and carotid arteries were collected and processed as described below.

2.2.3.3 Porcine coronary arteries stent implantation

Pigs were premedicated with aspirin (150 mg oral, Teva, Leeds, United Kingdom) and clopidogrel (150 mg oral, Sanofi-Aventis, Guildford, United Kingdom) over a 24-hours period before surgery. Pigs were sedated by an injection of tiletamine/zolazepam (100 mg Zoletil IM, Virbac, Suffolk, United Kingdom) and propofol (30 mg Rapinovet IV, Schering-Plough, Welwyn Garden City, United Kingdom). All animals were intubated and anesthesia maintained throughout the procedure using a mixture of isoflurane (1% to 2%, Abbott Laboratories Ltd., Maidenhead, UK) in oxygen/nitrous oxide. Unfractionated heparin (100 U/kg IV, Leo Laboratories, Bucks, United Kingdom) was given at the start of the procedure. Access to the coronary arteries was achieved via the left femoral artery, using standard 6 French sheaths and coronary guiding catheters. In the majority of animals, stents (Multi-Link Vision, 3.5 x 15 mm, Abbott) were placed in 2 of the 3 coronary arteries (left anterior descending, left circumflex, and right coronary arteries) under fluoroscopic guidance. Nine bindarit-treated animals (16 stents) and ten control animals (17 stents) were used for the morphometric analysis. Six bindarit-treated animals (12 stents) and six control animals (12 stents) were used for the proliferating cell nuclear antigen analysis. Five bindarit-treated animals (10 stents) and six control animals (12 stents) were used for evaluating the effect of bindarit on monocyte/macrophage infiltration. ECG and MAP were recorded continuously.

Stents were deployed at inflation pressures necessary to produce a stent to artery ratio of 1.2:1. After sheath removal, the femoral artery was ligated, and the leg wound was closed and sutured. All animals were given buprenorphine (0.15 mg of Vetergesic IM, Alstoe Ltd, York, United Kingdom) to provide analgesia and ampicillin (350 mg of Amfipen LA IM, Intervet, Welwyn Garden City, United Kingdom) for antibiotic cover, immediately after the procedure. Animals were recovered and received a normal diet, with supplementation of 75 mg of aspirin orally every 2 days and 75 mg of clopidogrel orally every 2 days for the duration of the study.

One control animal failed to develop vascular injury in both implanted stents and was excluded from the study. Pigs were euthanized 7 or 28 days after stent implantation, with an overdose of pentobarbital (200 mg/mL pentobarbitone, Merial, Harlow, United Kingdom) via the marginal ear vein, and the stented arteries were removed from the heart and flushed

with normal saline to remove non-adherent thrombus. The coronary arteries harvested 7 days after stent implantation were divided into 2 parts at the center of the stent. The proximal part was used for protein extraction, and the distal portion was fixed in 10% formaldehyde and used for immunohistochemical staining.

2.2.4 Tissue processing and Morphometric Analysis of Injured Arteries

For the evaluation of neointima formation, carotid arteries from rats or apoE$^{-/-}$ mice were fixed by perfusion with phosphate-buffered saline (PBS; pH 7.2) followed by PBS containing 4% formaldehyde through a cannula placed in the left ventricle. Paraffin-embedded sections were cut (6 μm thick) from the approximate middle portion of the artery and stained with haematoxylin and eosin. Ten sections from each carotid artery were reviewed and scored under blind conditions. The cross-sectional areas of media and neointima were determined by a computerized analysis system (LAS, Leica).

Stented coronary arteries harvested at 28 days were fixed in formal saline (24 hours) and dehydrated in pure acetone before resin embedding in glycol methacrylate (Technovit 8100, Kulzer, Wehrheim, Germany) following the manufacturer's instructions. Sections (4–12 in controls and 5–12 in bindarit) were obtained from the proximal to distal portion of the stent using a Buehler Isomet 1000 rotary precision saw (Buehler, Lake Bluff, IL) and mounted on a glass slide. Sections were then ground and polished using a Buehler Metaserv 2000 grinder to reduce the thickness to 10 μm and give a uniform surface for staining and microscopic evaluation. Sections were stained using hematoxylin/eosin to demarcate cell types, and images were acquired using a Leica DM LB2 microscope and Leica DFC320 digital camera. After digitalizing, histomorphometric measurements were performed with ImageJ (NIH Imaging, http://rsbweb.nih.gov/ij). Borders were manually traced for lumen area, area circumscribed by the internal elastic lamina (IEL), the border of the external elastic lamina (external elastic lamina area, vessel area) and stent circumference as the linear distance from strut to strut around the circumference of the stent (Suzuki T et al., 2001). The neointimal and medial areas were computed as follows: neointimal area = IEL area minus lumen area; medial area = external elastic lamina area minus IEL area. Furthermore, percentage area of stenosis was calculated as 100X (1 - lumen area/IEL area). Neointimal thickness (defined as the minimum distance between the strut and the lumen) was determined at each strut site and calculated as mean for each stented coronary segment. Results are expressed as the mean value from both stents per animal.

2.2.5 Injury and Inflammatory Score in Porcine Coronary Stent Model

The injury score was calculated as previously reported by Gunn J et al. (2002). Briefly, we considered both deep injury and stretch as follows: 0 = no impression of metal on media; 1 = deformation of the IEL by <45°; 2 = deformation of the IEL by >45°; 3 = rupture of the IEL; 4 = rupture of the external elastic lamina (that is complete medial rupture).

The inflammatory score was calculated as previously reported by Kornowski R et al. (1998) Briefly, we considered the extent and density of the inflammatory infiltrate in each individual strut, and the grading used was as follows: 0 = no inflammatory cells surrounding the strut; 1 = light, noncircumferential lymphohistocytic infiltrate surrounding the strut; 2 = localized, moderate to dense cellular aggregate surrounding the strut noncircumferentially; 3 = circumferential dense lymphohistiocytic cell infiltration of the strut. The injury and inflammatory score for each cross section were calculated as the sum of the individual injury or inflammatory scores, divided by the number of struts in the examined section.

2.2.6 Immunohistochemisty Analysis

2.2.6.1 Proliferating Cell Nuclear Antigen (PCNA) Analysis in Injured Arteries

Proliferating cell nuclear antigen (PCNA) analysis was used to quantify the proliferative activity of cells at the injury sites.

After fixation in 10% formaldehyde of the coronary arteries harvested at day 7, the stent struts were gently removed with micro-forceps under a dissection microscope. The specimens were dehydrated, embedded in paraffin, and cut into 7-μm-thick slices.

After antigen retrieval in citrate buffer, the sections from rat or mouse apoE$^{-/-}$ carotid arteries and porcine coronary arteries, were incubated with monoclonal mouse anti-PCNA antibody (1:250, PC10, Sigma) and biotinylated anti-mouse secondary antibody (1:200, DakoCytomation, Milan, Italy). Slides were treated with streptavidin– horseradish peroxidase (DakoCytomation) and exposed to diaminobenzidine chromogen (DakoCytomation) with hematoxylin counterstain.

Six sections from each rat carotid artery and ten random fields per section were reviewed and scored under blind conditions. Data are expressed as the percentage of total arterial (medial plus neointimal) PCNA positive cells 7 days after angioplasty.

Ten sections from each mouse apoE$^{-/-}$ carotid artery were reviewed and scored under blind conditions. Results are expressed as percentage of total PCNA-positive cells 7 days after wire injury.

Ten sections from each porcine coronary artery and ten random fields (X 20 objective) per section were reviewed and scored under blind conditions. Data are expressed as the percentage of total PCNA positive cells 7 days after stent implantation.

2.2.6.2 MCP-1 Immunoistochemistry in rat injured carotid arteries

Rat carotid arteries (1, 7, and 14 days after angioplasty, or naive) were snap-frozen in liquid nitrogen in OCT embedding medium (Tissue Tek, Sakura Finetek). Ten cross-sections were cut (6 mm) from the approximate middle portion of the artery and used for MCP-1 detection. Sections were incubated with polyclonal goat anti-MCP-1 antibody (1:50, R-17, Santa Cruz) diluted in blocking buffer/0.3% Triton X-100 (MP Biomedicals) in PBS overnight before being washed in TNT wash buffer (Tris–HCl, pH 7.5, 0.15 M NaCl, and 0.05% Tween 20; Sigma). Sections incubated with goat nonimmune serum were used as negative controls. Subsequently, sections were incubated with biotinylated anti-goat secondary antibody (1:400, DakoCytomation) diluted in blocking buffer/0.3% Triton X-100, washed in TNT wash buffer, treated with streptavidin–HRP, and exposed to diaminobenzidine chromogen with haematoxylin counterstain. The sections were photographed and the images were stored in the image analysis system (LAS, Leica).

2.2.6.3 Immunohistochemisty analysis in injured apoE$^{-/-}$ mouse carotid arteries

Carotid arteries were snap-frozen in liquid nitrogen in OCT embedding medium. Fifteen cross-sections were cut (6 mm) from the approximate middle portion of the artery and used for MCP-1, a-smooth muscle actin (a-SMA), and macrophage detection by immunofluorescence. For staining, the sections were processed as described above and incubated with polyclonal goat anti-mouse MCP-1 antibody (1:50, M-18, Santa Cruz) or rat anti-F4/80 monoclonal antibody (1:50, clone BM8, Abcam) diluted in blocking buffer/0.3% Triton X-100 (MP Biomedicals) in PBS overnight before being washed in TNT wash buffer. Sections incubated with non-immune goat serum or an isotype-matched control antibody were used as negative controls. Subsequently, the sections were incubated with 1:75 Texas Reddonkey anti-goat IgG (Jackson ImmunoResearch Laboratories) or with 1:200 biotinylated anti-rat secondary antibody (DakoCytomation), amplified with Tyramide Signal Amplification Systems (PerkinElmer), and revealed with streptavidin–FITC (1:50, DakoCytomation). Monoclonal anti-α-SMA FITC (1:250, clone 1A4, Sigma) was added in blocking buffer for 1 hour before washing as described above. DAPI was used to identify nuclei. Images were taken using an AxioCam HRc videocamera (Zeiss) connected to an

Axioplan fluorescence microscope (Zeiss) using the AxioVision 3.1 software. The neointimal areas stained for F4/80 were determined in digitized images (five sections per mouse), and positive areas for specific immunostaining were quantified (NIH Imaging; http://rsb .info.nih.gov/ij). Data are expressed as the percentage of the immunostained area per total neointimal area. Serial carotid paraffin-embedded sections were cut (5 mm) and used for detection of calponin (1:100, clone hCP, Sigma). Ten sections from each carotid artery were reviewed and scored under blind conditions. The number of calponin-positive cells in neointima was counted.

2.2.6.4 Contractile Proteins Localization in rat carotid arteries

Paraffin sections (6 μm) from rat carotid arteries (7, 14 and 28 days after angioplasty, or naïve animals) were deparaffinised and endogenous peroxidase activity was blocked by incubating with 0.3% H_2O_2 following antigenic recovery. The sections were incubated with the primary antibody against α-SMA (1:100), calponin (1:50) or SMemb (1:200) diluted in blocking buffer/0.3% Triton X-100 (MP Biomedicals) in PBS overnight before being washed in TNT wash buffer (Tris–HCl, pH 7.5, 0.15 M NaCl, and 0.05% Tween 20; Sigma). Sections incubated with isotype matched antibodies were used as negative controls. Subsequently, sections were incubated with biotinylated anti-mouse (1:500, DakoCytomation) diluted in blocking buffer 0.3% Triton X-100, washed in TNT wash buffer, treated with horseradish peroxidise labelled streptavidin, and exposed to diaminobenzidine chromogen with haematoxylin counterstain. The sections were photographed and the images were stored in the image analysis system (LAS, Leica).

2.2.7 Evaluation of re-endothelialization in injured rat carotid arteries

Re-endothelialization was assessed 2 weeks after balloon injury by staining with Evans Blue dye (0.5 mL of 0.5% Evans Blue dye iv; Sigma) as described previously (Asahara T et al., 1996). Planimetric analysis with an image analysis program (LAS, Leica) was performed. Re-endothelialization was expressed as the percentage of re-endothelialized area vs the total denuded area. To verify that the Evans Blue stain accurately depicted the presence or absence of endothelium, sections of completely or partially re-endothelialized carotid arteries (based on Evans Blue appearance) were stained with antibody to von Willebrand factor (vWF, Cytomation Dako) as described previously (Yue TL et al., 2000).

2.2.8 Total Tissue Extracts

All the extraction procedures were performed on ice with ice-cold reagents. Briefly, frozen porcine coronary arteries or pooled carotid arteries (n = 2), were crushed into a fine powder in a mortar with a pestle under liquid nitrogen and resuspended in an adequate volume of Cell Extraction Buffer containing 100 mmol/L Tris, pH 7.4; 2 mmol/L Na3VO4; 100 mmol/L NaCl; 1% Triton X-100; 1 mmol/L EDTA; 10% glycerol; 1 mmol/L EGTA; 0.1% SDS; 1 mmol/L NaF; 0.5% deoxycholate; 20 mmol/L Na4P2O7, supplemented with 1 mmol/L phenylmethylsulfonyl fluoride and Protease Inhibitor Cocktail (P2714) (Sigma, Dorset, United Kingdom) just before use and then centrifuged at 13000xg at 4 °C for 30 minutes. Supernatant were transferred to fresh tubes and stored at -80 °C until the assays. Protein concentration was determined using the Bio-Rad protein assay kit (Bio-Rad).

2.2.9 Western blot Analysis on Injured Arteries

The levels of PCNA and CD68 expression in total protein extracts from porcine coronary arteries were evaluated respectively 7 and 28 days after stent implantation. Equivalent amounts of protein (60 μg) from each sample were electrophoresed on a 10% discontinuous polyacrylamide gel.

The levels of PCNA, CD68, α-SMA, calponin and SMemb were evaluated in total extracts from rat carotid arteries 7, 14, and 28 days after injury. Equivalent amounts of protein (50 μg) from each sample were electrophoresed on a 10% discontinuous polyacrylamide gel.

After incubation with a primary antibody against PCNA (1:2000, Sigma-Aldrich), mouse anti-CD68 (1:1000, AbD Serotec), α-SMA (1:5000), calponin (1:3000) or SMemb (1:2000), the membranes were washed and incubated with anti-mouse immunoglobulins coupled to peroxidase (1:2000). The immunocomplexes were visualised by the ECL chemiluminescence method and results were normalized to of the housekeeping protein β-actin or glyceraldehyde-3-phosphate dehydrogenase (GAPDH).

2.2.10 ELISA on animal tissues

Rat carotid artery was crushed into powder and resuspended in 100 mL of lysis buffer (20 mM HEPES, 0.4 mM NaCl, 1.5 mM MgCl2, 1 mM EGTA, 1 mM EDTA, 1% Triton X-100, and 20% glycerol) with protease inhibitors (1 mM DTT, 0.5 mM PMSF, 15 mg/mL Try-inhibitor, 3 mg/mL pepstatin-A, 2 mg/mL leupeptin, and 40 mM benzamidine). After centrifugation at 13 000 g at 48C for 30 min, MCP-1 in the supernatants was quantified

using an ELISA kit (OptEIATM, Biosciences). All measurements were performed in duplicate. The values were corrected by protein concentrations measured by the Bio-Rad protein assay kit (Bio-Rad). Serum MCP-1 levels (1, 7, and 14 days after angioplasty) were also measured in the same animals used above by ELISA (OptEIATM, Biosciences). The results are expressed as nanograms per millilitre. MCP-1 levels in rat carotid arteries 1, 7, and 14 days after balloon injury was quantified using an ELISA kit according to the manufacturer's instructions (OptEIATM, Biosciences). All measurements were performed in duplicate. The values were corrected by protein concentrations measured by the Bio-Rad protein assay kit (Bio-Rad).

MCP-1, total cholesterol, and triglyceride serum levels were also determined in apoE$^{-/-}$ mice 28 days after wire injury, using enzymatic immunoassays according to the manufacturer's instructions (OptEIATM, Biosciences; Serum Triglyceride Kit, Sigma; Cholesterol Assay Kit, Cayman Chemical). The results are expressed as pg/mL and mg/dL respectively.

MCP-1 plasma levels were measured in pigs 28 days after stent implantation by ELISA according to the manufacturer's instructions (Pig CCL-2 ELISA kit, Bethyl Laboratories, Montgomery, TX). The results are expressed as pg/mL

2.2.11 Statistical Analysis

Results are expressed as mean±SEM of n animals for in vivo experiments and mean±SEM of multiple experiments for in vitro assays. Student's t-test was used to compare two groups and ANOVA (two tailed P-value) was used with the Dunnett post hoc test for multiple groups using Graph Pad Instat 3 software (San Diego, CA, USA). The level of statistical significance was 0.05 per test.

3. RESULTS

3.1 Effect of bindarit on neointima formation in both rats and hyperlipidaemic mice

3.1.1 Rat VSMC Proliferation and Migration

Initiation and maintenance of SMCs proliferation is a critical event in the pathogenesis of neointima formation. As shown in Figure 6A, bindarit at 100 and 300 μM significantly inhibited PDGF-BB-induced rat SMCs proliferation by 27% ($P<0.05$, n = 3) and 42% ($P<0.01$, n = 3), respectively. Similar results were obtained with apoE$^{-/-}$ mice VSMC (data not shown). Another key mechanism of neointima formation is mitogen-mediated migration of SMCs. Therefore, we evaluated the effects of bindarit on PDGF-BB-induced rat SMCs chemotaxis. Bindarit inhibited significantly ($P<0.01$, n = 3) chemotactic migration at 100 and 300 μM by 45 and 50%, respectively (Figure 6B). Moreover, bindarit (100 μM) also significantly reduced rat SMCs invasion (by 30%, $P<0.01$, n = 3, Figure 6C) through the Matrigel barrier which mimics extracellular matrix. Analysis of cell viability (>95%) demonstrated that it was not affected by bindarit at the concentrations used in this study (data not shown).

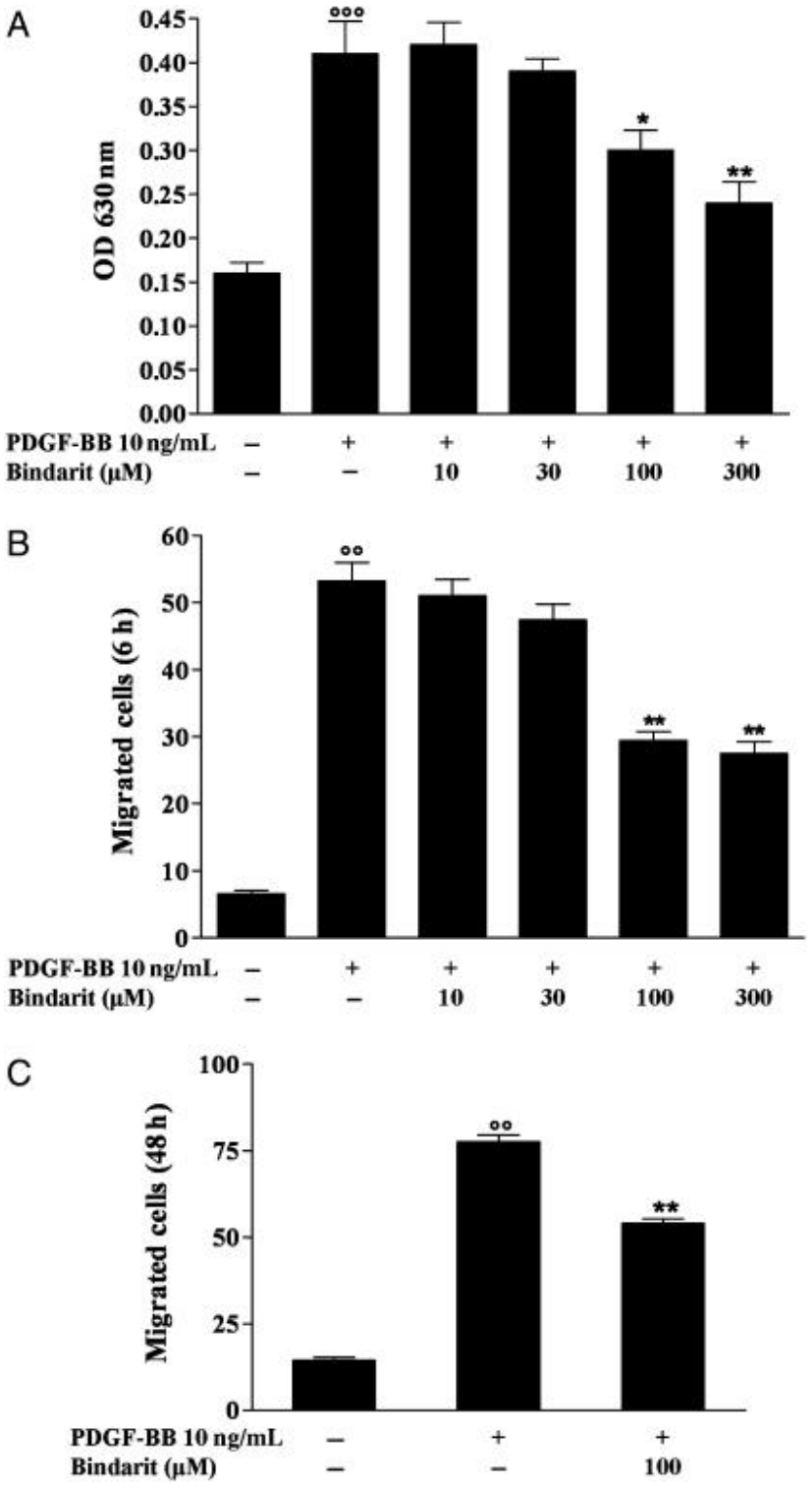

Figure 6

(*A*) Effect of bindarit (10-300 μM) on rat SMC proliferation, (*B*) migration, and (*C*) invasion performed as described above. Results are expressed as mean±SEM from three separate experiments. **P*<0.05, ***P*<0.01 *vs* platelet derived growth factor-BB (PDGF-BB); °°*P*<0.01, °°°*P*<0.001 *vs* unstimulated cells.

3.1.2 MCP-1 Production in rat SMC

To determine whether the anti-proliferative and anti-migratory effects of bindarit were associated with MCP-1 inhibition, protein concentration of MCP-1 in the supernatant of cultured rat SMCs was determined by ELISA. As shown in Table 1, stimulation of SMCs with PDGF-BB (10 ng/mL) caused a time-dependent increased release of MCP-1 compared with that observed in unstimulated cells. When rat SMCs were stimulated with PDGF-BB in the presence of bindarit (10-300 μM), a concentration-related inhibition of MCP-1 production was observed.

	MCP-1 (ng/mL)			
	6 h	12 h	24 h	48 h
Unstimulated cells	0.32 ± 0.02	3.2 ± 0.21	18.5 ± 0.9	34.1 ± 1.4
PDGF-BB 10 ng/mL	3.1 ± 0.1°°	20.8 ± 1.58°°	59.6 ± 0.4°°	142.6 ± 2.8°°
+ bindarit 10 μM	3.0 ± 0.2	18.3 ± 1.2	50.9 ± 1.2**	128.0 ± 3.7**
+ bindarit 30 μM	1.5 ± 0.1**	13.7 ± 0.5**	42.8 ± 0.6**	87.3 ± 1.7**
+ bindarit 100 μM	1.3 ± 0.2**	11.9 ± 0.4**	34.0 ± 1.0**	80.1 ± 1.8**
+ bindarit 300 μM	0.8 ± 0.1**	4.8 ± 0.5**	29.3 ± 1.1**	72.1 ± 1.3**

Table 1
Effect of bindarit on MCP-1 production by platelet derived growth factor-BB (PDGF-BB)-stimulated SMCs. Results are expressed as mean+SEM of three separate experiments performed in triplicate. °°P<0.01 *vs* unstimulated cells.**P<0.01 *vs* PDGF-BB.

3.1.3 Neointima Formation in rat carotid arteries

To determine the efficacy of a systemic treatment with bindarit for the limitation of neointimal hyperplasia, a rat carotid arterial injury model was used. A remarkable increase in the number of PCNA-positive cells was demonstrated in both the media and neointima 7 days after injury in control rats, which was significantly reduced (P<0.001, n = 9) in the bindarit-treated group (200 mg/kg/day) by 54 and 30%, respectively (Figure 7A). Bindarit caused a significant inhibition of neointima formation by 39% (P<0.01, n = 19) at day 14 compared with the control animals (Figure 7B). Medial area (0.124±0.003 mm^2 in the sham group) was not affected by both vascular injury and bindarit.

3.1.4 Monocytes/Macrophages Infiltration in rat carotid arteries

Western blot analysis was performed to examine the effect of bindarit on the carotid monocyte/macrophage content. Monocyte/macrophage marker CD68 was highly expressed in carotid arteries 14 days after angioplasty when compared with that of sham-operated animals (Figure 7C). Bindarit significantly reduced CD68 levels as shown by relative densitometric analysis.

3.1.5 MCP-1 Production in rat carotid arteries

We observed a significant time-dependent increase in MCP-1 production in the injured arteries at 1, 7, and 14 days after angioplasty when compared with that of sham-operated animals (Figure 7D). Bindarit was able to inhibit the MCP-1 protein expression throughout the time course considered, by 31% ($P<0.05$; n = 5), 38% ($P<0.05$; n = 5), and 49% ($P<0.001$; n = 5) at 1, 7, and 14 days after injury, respectively. In the contralateral carotid artery, no significant changes were observed throughout the observation period compared with those measured in sham-operated animals. In carotid arteries from naïve animals, the levels of MCP-1 measured were 0.74±0.34 ng/mg (n = 5).

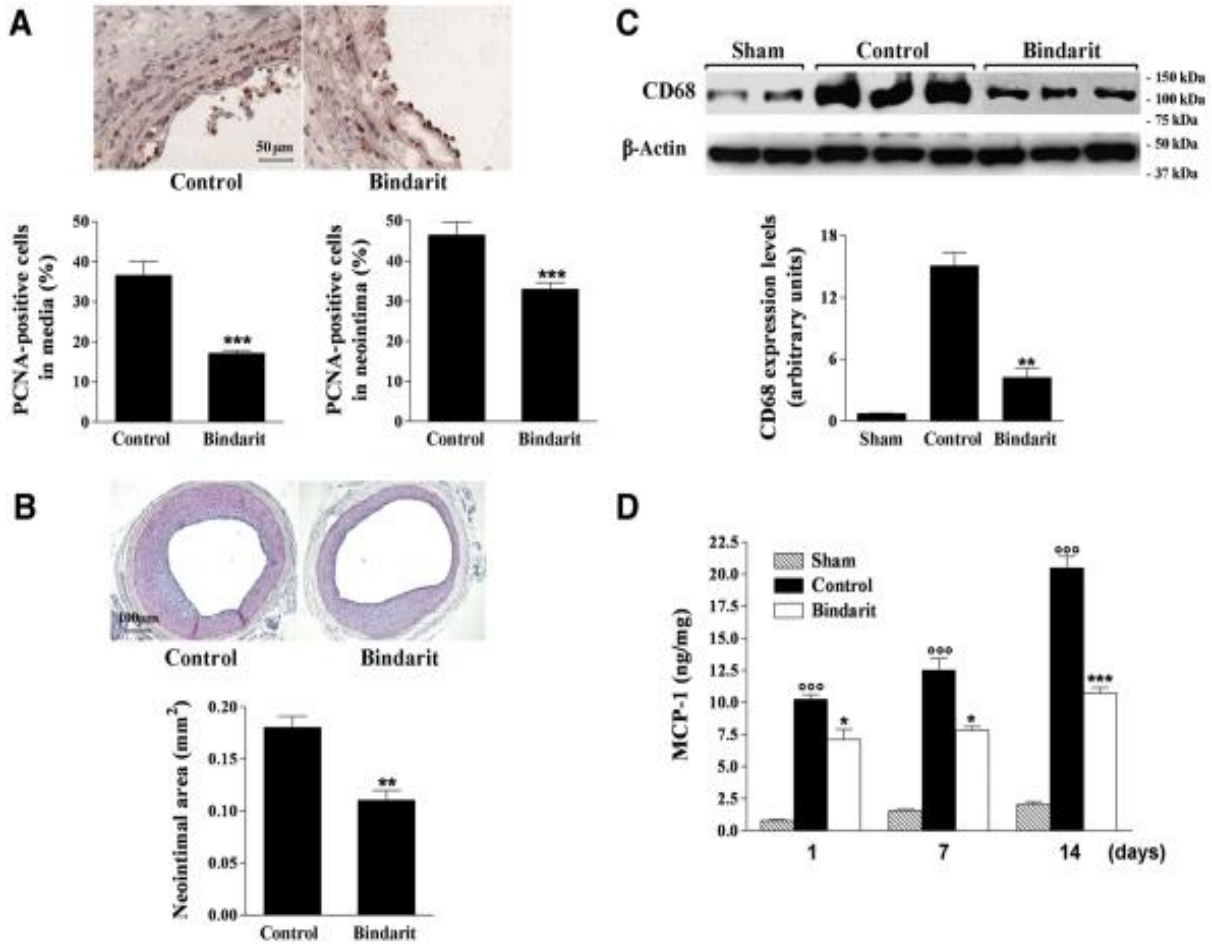

Figure 7

(*A*) Photomicrographs showing the effect of bindarit (200 mg/kg/day) on PCNA-positive cells in rat carotid arteries at day 7 after injury (magnification ×400). Results are expressed as mean±SEM of the percentage of total medial and neointimal cells positive for PCNA, where n = 9 rats for each group. ***P<0.001 *vs* control group. (*B*) Photomicrographs showing the effect of bindarit (200 mg/kg/day) on neointima formation in rat carotid arteries 14 days after balloon injury (magnification ×100). Results are expressed as mean±SEM, where n = 15-19 rats. **P<0.01 *vs* control group. (*C*) Effect of bindarit (200 mg/kg/day) on monocyte/macrophage marker CD68 protein expression in carotid arteries 14 days after angioplasty. Equal loading was confirmed by β-acting staining. Results are expressed as mean±SEM of three separate experiments. **P<0.01 *vs* control group. (*D*) Effect of bindarit (200 mg/kg/day) on MCP-1 expression in rat carotid arteries 1, 7, and 14 days after balloon injury evaluated by ELISA. Results are expressed as mean±SEM of MCP-1 levels normalized with protein concentrations, where n = 5. *P<0.05; ***P<0.001 *vs* control group; °°°P<0.001 *vs* sham-operated animals.

3.1.6 MCP-1 Localization in rat carotid arteries

Non-injured carotid arteries lacked immunoreactivity for MCP-1, whereas injured arteries stained strongly for MCP-1 (Figure 8). Negative controls showed no signal. MCP-1-positive staining was detectable in media of injured vessel from days 1 up to 14 and in neointimal cells at days 7 and 14. MCP-1 localization was not modified by bindarit, whereas the drug treatment resulted in a lower MCP-1 expression in both media and neointima (Figure 8).

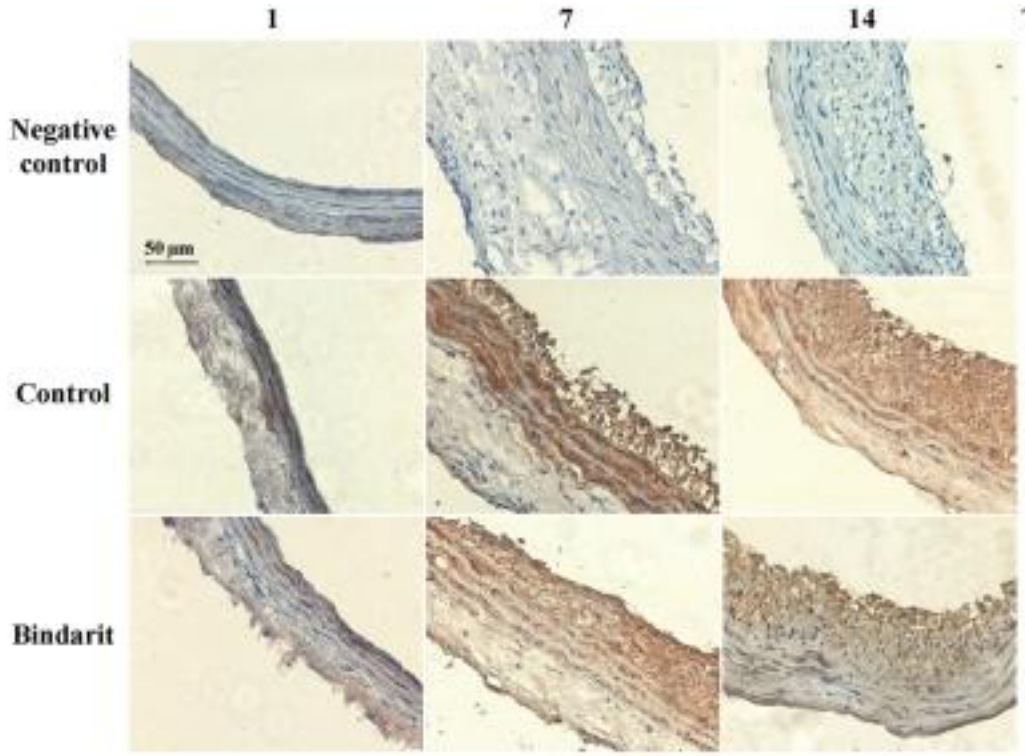

Figure 8
Immohistochemical localization of MCP-1 expression in rat carotid arteries 1, 7, and 14 days after angioplasty.

3.1.7 Re-endothelialization in rat carotid arteries

Evans Blue staining identifies segments of injured carotid arteries that have not been re-endothelialized. As shown in Figure 9, the presence of intact endothelium in the carotid artery of naïve rats was demonstrated by the absence of Evans Blue staining. Immunohistochemical staining with antibody to vWF verified the presence of endothelium. In contrast, the entire area of the artery harvested 1 day after injury was stained by Evans Blue. The absence of positive staining with antibody to vWF confirmed the observation. Analysis of samples at 2 weeks from angioplasty showed that bindarit treatment did not affect re-endothelialization of arteries when compared with control animals.

3.1.8 MCP-1 Serum Levels in rats

A time-dependent increase in MCP-1 serum concentration was observed in rats subjected to angioplasty (Table 2). Bindarit caused a significant inhibition of MCP-1 serum levels at day 1 by 20% ($P<0.05$, n = 10) and at days 7 and 14 by 30% ($P<0.001$, n = 10) compared with their respective control groups. In naïve animals, the MCP-1 serum level was 29.4±3.0 ng/mL (n = 5).

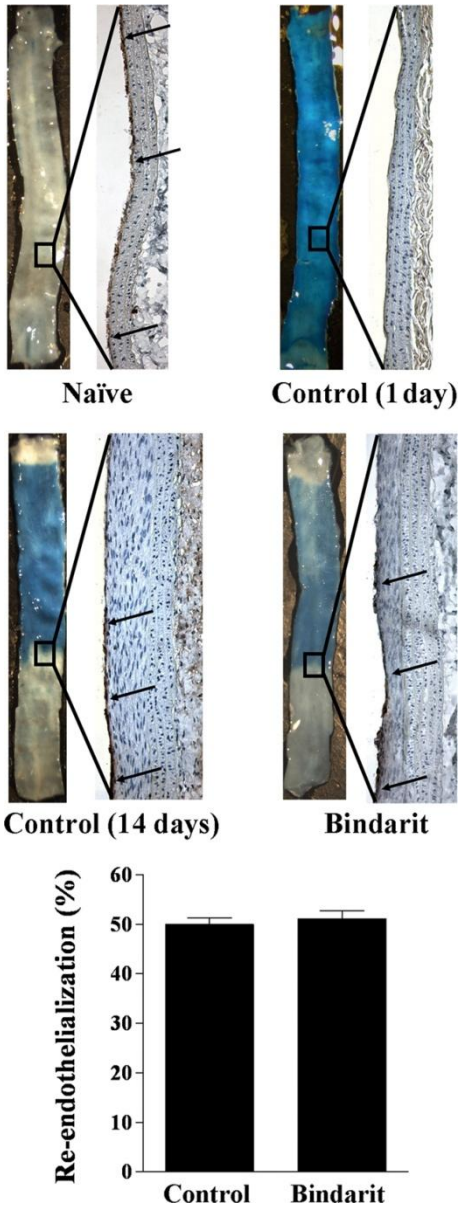

Figure 9
Extent of re-endothelialization in injured carotid arteries evaluated by Evans Blue staining. Representative arteries harvested from naïve animals, as well as 1 and 14 days after carotid injury in vehicle- or bindarit-treated rats. Evans Blue staining identifies segments of each artery that have not been recovered by endothelium. Immunohistochemical staining with antibody to vWF verified the presence of endothelium. Re-endothelialization was expressed as the percentage of re-endothelialized area *vs* the total denuded area (bottom panel) (n = 5).

Group	MCP-1 (ng/mL)		
	1-day	7-day	14-day
Sham-operated	37.1 ± 2.4	35.4 ± 1.2	32.8 ± 2.7
Control	69.2 ± 3.5°°	51.4 ± 2.2°°	53.7 ± 3.9°°
Bindarit 200 mg/kg/day	55.6 ± 3.0*	36.2 ± 2.4***	37.2 ± 2.1***

Table 2
Effect of bindarit on MCP-1 serum levels in rats. Results are expressed as mean±SEM, where *n* = 5–10 rats per each time point considered. °°*P*<0.01 vs. sham-operated animals.*$P<0.05$; ***$P<0.001$ *vs* control group.

3.1.9 Neointima Formation in apoE$^{-/-}$ mice

To evaluate the effect of bindarit after arterial injury in hyperlipidaemic animals, carotid endothelial denudation was performed in apoE$^{-/-}$ mice fed an atherogenic diet. Seven days after injury, the number of PCNA-positive cells was significantly reduced (42%, $P<0.05$, n = 10) by treatment with bindarit (200 mg/kg/day) compared with control mice (Figure 10A). Neointimal area was reduced by 47% in apoE$^{-/-}$ mice treated with bindarit compared with control mice 28 days after injury (Figure 10B). Moreover, the apoE$^{-/-}$ mice receiving bindarit showed a 66% reduction in the relative content of F4/80-positive macrophages and a 30% reduction in the number of SMCs in neointimal lesion (Figure 10C and 10D).

Injured carotid arteries stained strongly for MCP-1 detectable in media and neointima 28 days after injury. Co-localization of MCP-1 and α-actin was evident in both media and neointima. MCP-1 localization was not modified by bindarit, but again the drug reduced both medial and neointimal MCP-1 expression (Figure 10E).

Total cholesterol levels did not differ between groups (1036±38 mg/dL in bindarit-treated group, n=10 *vs* 1167±50 mg/dL in control group, n = 10), whereas triglyceride levels were significantly lower ($P<0.05$) in bindarit-treated animals (191.6±21.3 mg/dL, n = 10) than in the control group (260.7±20.6 mg/dL, n = 10). Moreover, bindarit caused a significant inhibition ($P<0.01$) of MCP-1 serum levels by 42% (131.0±15.6 pg/mL in bindarit-treated group, n = 10 *vs* 224.8±28.3 pg/mL in control group, n = 10; $P<0.01$).

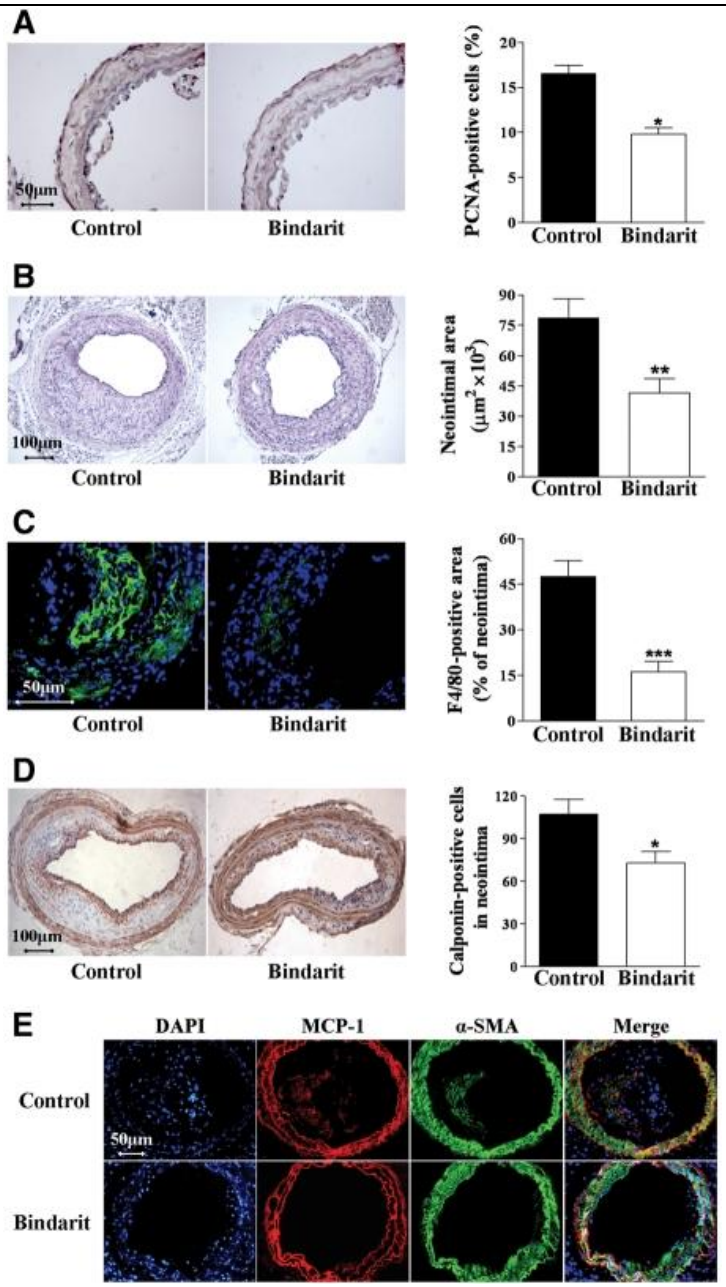

Figure 10

(*A*) Photomicrographs showing the effect of bindarit (200 mg/kg/day) on PCNA-positive cells in apoE$^{-/-}$ mice 7 days after injury (magnification ×400). Results are expressed as mean±SEM of the percentage of total PCNA-positive cells, where n = 10 rats for each group. **P*<0.05 *vs* control group. (*B*) Photomicrographs showing the effect of bindarit (200 mg/kg/day) on neointima formation in apoE$^{-/-}$ mice 28 days after carotid injury (magnification ×100). Results are expressed as mean±SEM, where n = 10 for each group; ***P*<0.01 *vs* control group. (*C*) Photomicrographs showing the effect of bindarit (200 mg/kg/day) on macrophage content in carotid arteries 28 days after injury (magnification ×400). Results are expressed as mean±SEM of the percentage of F4/80 immunostained area per total neointima area, where n = 10 for each group; ****P*<0.001 *vs* control group. (*D*) Photomicrographs showing the effect of bindarit (200 mg/kg/day) on neointimal SMCs content in carotid arteries 28 days after injury (magnification ×100). Results are expressed as mean±SEM of the calponin-immunostained cell number, where n = 10 for each group; **P*<0.05 *vs* control group. (*E*) Immunofluorescence visualization of α-SMA (green) and MCP-1 (red) in mouse carotid arteries 28 days after injury. DAPI (blue) was used to locate nuclei. Co-localization of MCP-1 and α-actin (yellow) was evident in some cells in both media and neointima (magnification ×200)

3.2 Effect of bindarit on in-stent stenosis in porcine coronary arteries

3.2.1 Morphometric Analysis

Representative stented artery sections obtained 28 days after implantation are shown in Figure 11. Morphometric assessment showed a significant reduction in neointimal area (4.03±0.46 *vs* 6.65±0.44 mm^2, $P<0.001$) (Figure 12A), neointimal thickness (270.2±26.92 *vs* 551.06±49.94 μm, $P<0.001$) (Figure 12B), percentage of stenosis (47.56±3.42% *vs* 74.97±2.71%, $P<0.001$) (Figure 12C), and inflammatory score (1.10±0.06 *vs* 1.83±0.11, $P<0.001$) (Figure 12D) in the bindarit-treated group compared with control animals. Moreover, in the bindarit-treated group, the lumen area was significantly increased compared with the control group (4.43±0.33 *vs* 2.12±0.15 mm^2, $P<0.001$) (Figure 2E). No significant differences were detectable in vessel area (10.48±0.56 *vs* 11.05±0.35 mm^2), IEL area (8.47±0.50 *vs* 8.76±0.31 mm^2), or medial area (2.01±0.08 *vs* 2.28±0.14 mm^2). Importantly, there was no significant difference in the injury score (2.31±0.11 *vs* 2.23±0.13) (Figure 12F) and stent circumference (9.53±0.16 *vs* 9.55±0.28 mm^2) between the 2 groups, indicating and that experimental and control animals had a similar degree of injury and complete stent deployment.

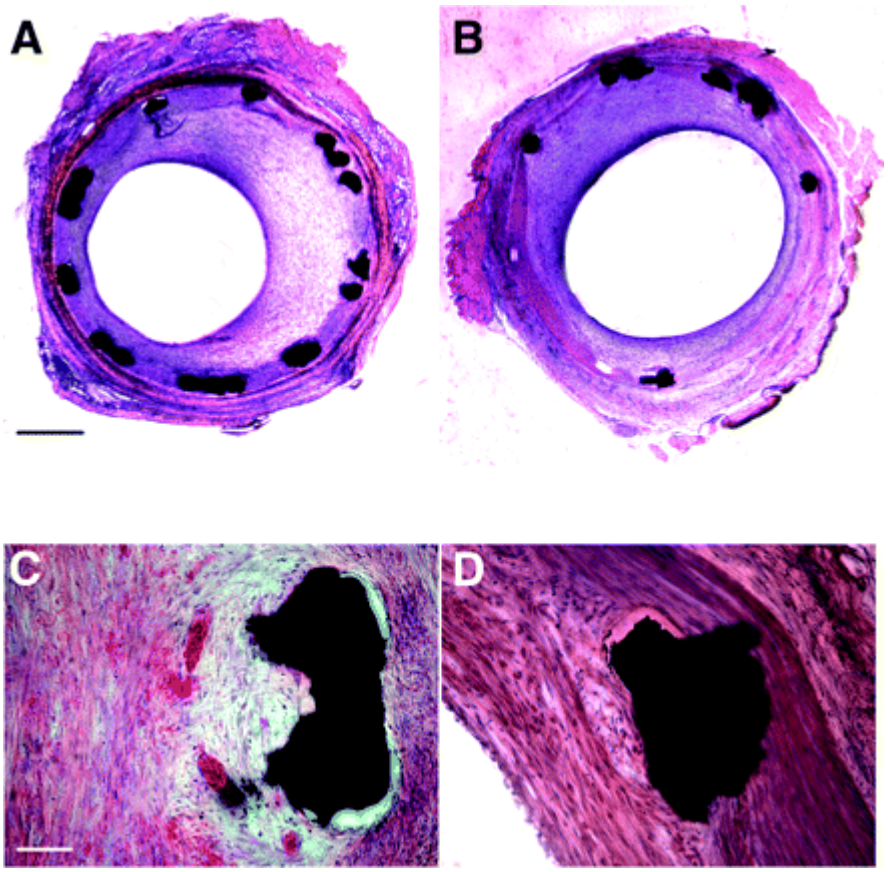

Figure 11
A and B, Representative photomicrographs (hematoxylin/eosin staining) showing the effect of bindarit on in-stent stenosis 28 days after stent deployment (A: control group; B: bindarit). Scale bar = 1 mm. C and D, Representative photomicrographs showing the reduction in inflammatory cell influx in the bindarit-treated group (D) *vs* control group (C). Scale bar = 100 µm

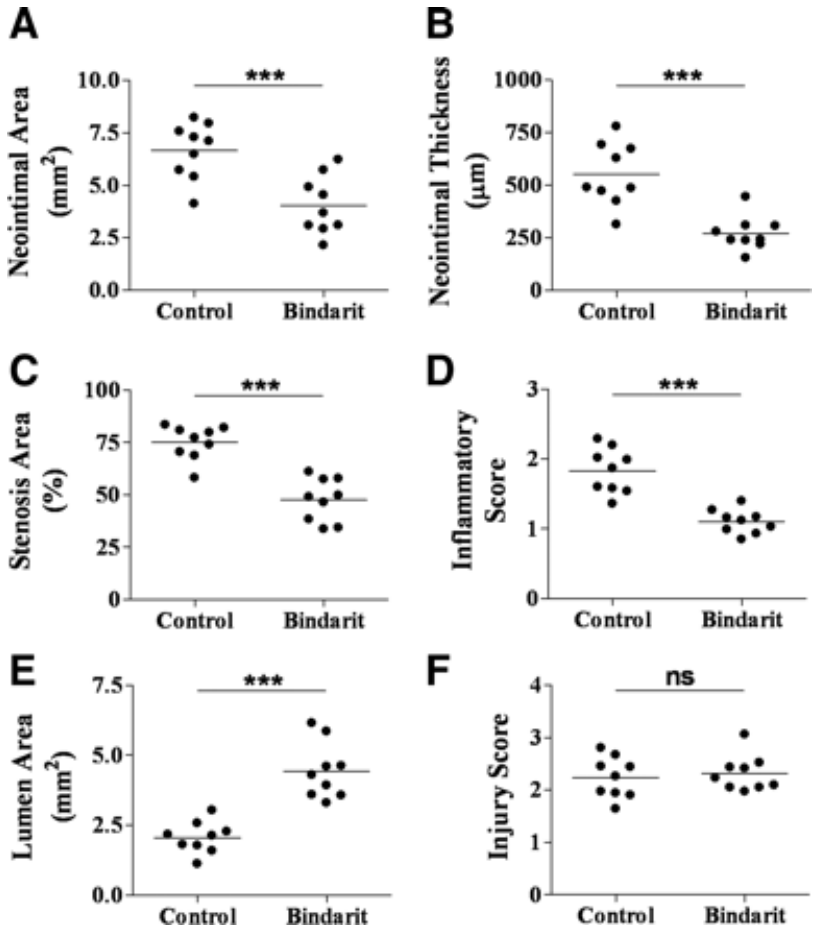

Figure 12
Effect of bindarit on neointimal area (A), neointimal thickness (B), percentage of stenosis (C), inflammatory score (D), lumen area (E), and injury score (F). Data per single animal and means (bars) are presented. ***P<0.001 *vs* control group. ns indicates not significant.

3.2.2 In Vivo Proliferation

Treatment with bindarit significantly reduced (by 45%, P<0.05) the number of PCNA-positive cells in the artery 7 days after stent implantation compared with control group (Figure 13A and 13B). Results were also confirmed by Western blot analysis. (Supplemental Figure I, available online at http://atvb.ahajournals.org).

3.2.3 Monocyte/Macrophage Infiltration in porcine coronary arteries

Western blot analysis was performed to examine the effect of bindarit on the monocyte/macrophage infiltration. The monocyte/ macrophage marker CD68 was highly expressed in coronary arteries 28 days after stent implantation. Bindarit significantly

reduced (by 55%, $P<0.01$) CD68 levels as shown by relative densitometric analysis (Figure 13C and 13D).

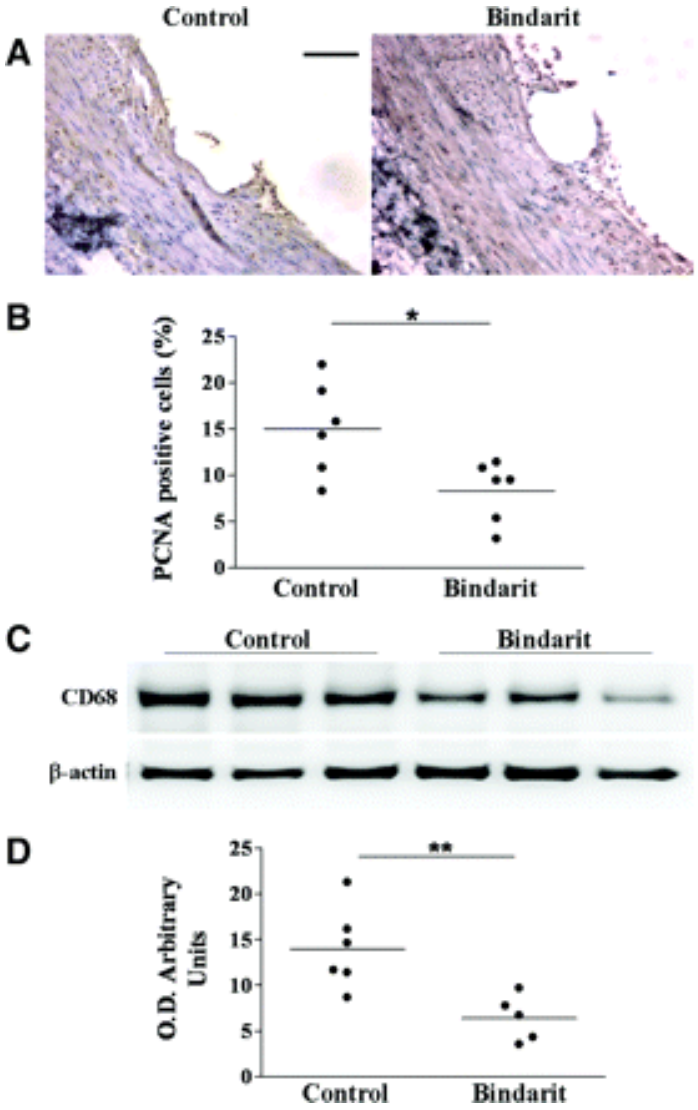

Figure 13
(A) Representative photomicrographs of proliferating cell nuclear antigen (PCNA)–stained coronary arteries at day 7 after stent implantation (magnification ×200). Scale bar = 100 μm. (B) Graph showing the effect of bindarit on cell proliferation in vivo. Results are expressed as percentage of total arterial (medial plus neointimal) cells positive for PCNA, as described in Methods. Data per single animal and means (bars) are presented. (C) Representative blot showing the effect of bindarit on CD68 expression in the protein extract of single coronary arteries 28 days after stenting. (D) Densitometric analysis of CD68 expression levels normalized to protein levels of β-actin. Data per single animal and means (bars) are presented. *$P<0.05$ and **$P<0.01$ *vs* control group.

3.2.4 MCP-1 Plasma Levels in pigs

A significant increase (P<0.01) in MCP-1 plasma concentration was observed in pigs subjected to stenting compared with the naïve animals (1903.05±172.64 pg/mL, n = 9, *vs* 885.41±26.74 pg/mL, n = 5). Bindarit caused a significant (P<0.05) inhibition of MCP-1 plasma levels at day 28 by ≈30% (1369.45±76.13 pg/mL, n = 7) (Figure 14).

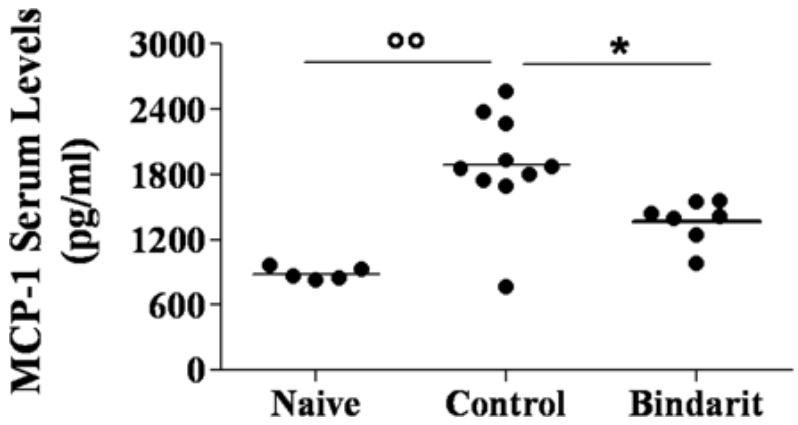

Figure 14
Effect of bindarit on monocyte chemotactic protein-1 (MCP-1) plasma levels in pigs 28 days after stent implantation. °°P<0.01 vs naïve animals, *P<0.05 vs control group.

3.2.5 Porcine SMC Proliferation

As shown in Figure 15, bindarit at 100 and 300 μmol/L significantly inhibited TNF-α-induced porcine SMC proliferation by 33% band 50% (P<0.01, n = 3), respectively. Cell viability (>95%) was not affected by bindarit at the concentrations used in this study (data not shown).

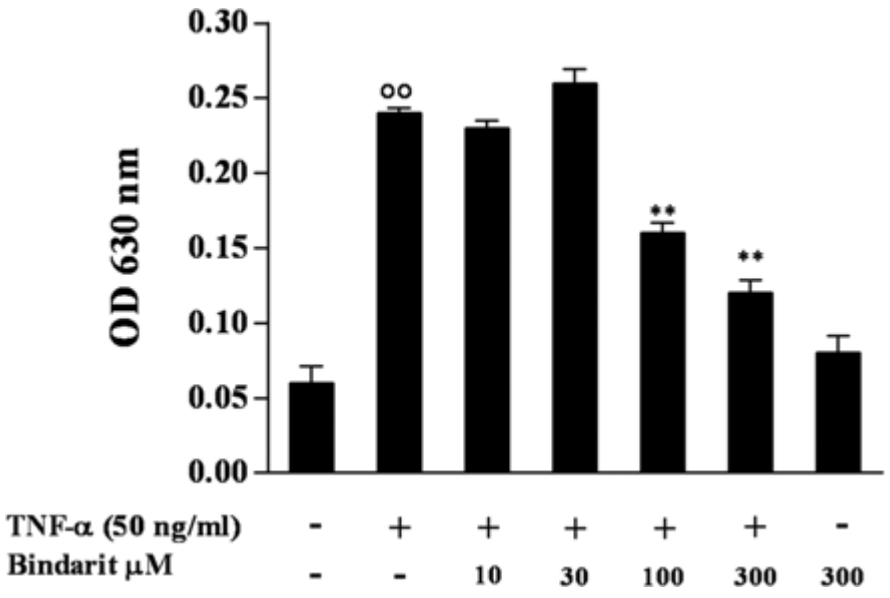

Figure 15
Effect of bindarit (10-300 μmol/L) on tumor necrosis factor-α (TNF-α)–induced porcine smooth muscle cell proliferation. Results are expressed as mean±SEM of three separate experiments run in triplicate. °°P<0.01 *vs* unstimulated cells, **P<0.01 vs TNF-α.

3.2.6 MCP-1 Production in porcine SMC

To determine whether the in vitro antiproliferative effect of bindarit was associated with MCP-1 inhibition, MCP-1 protein concentration was determined by ELISA in the supernatants of cultured primary porcine SMCs. As shown in the Table 3, stimulation of SMCs with TNF-α (50 ng/mL) caused an increase in release of MCP-1 compared with unstimulated cells. When porcine SMCs were stimulated with TNF-α in the presence of bindarit (10–300 μmol/L), a significant inhibition of MCP-1 production was observed at 100 and 300 μmol/L.

	MCP-1 (pg/mL)			
	12 h	24 h	48 h	72 h
Unstimulated cells	242±32	1044±77	1906±150	2520±164
TNF-α 50 ng/mL	1840±192*	3817±215*	5120±220*	5354±161*
+ bindarit 10 μmol/L	1637±123	3450±199	5450±310	6030±358
+ bindarit 30 μmol/L	1701±51	3920±257	4770±353	5389±266
+ bindarit 100 μmol/L	1241±55†	3046±152‡	4080±144‡	3782±116†
+ bindarit 300 μmol/L	1088±36†	2430±133†	3400±174†	2824±110†

Table 3
Effect of bindarit on MCP-1 Production by TNF-α-Stimulated Porcine SMC. Results are expressed as mean±SEM of three experiments run in triplicate. *P<0.01 *vs* unstimulated cells.†P<0.01 *vs* TNF-α; ‡P<0.05 *vs* TNF-α.

3.3 Effect of Bindarit on Human CASMC Proliferation, Migration and Phenotypic Switching

3.3.1 Contractile Proteins Expression in CASMCs

CASMCs were stimulated with TNF-a (30 ng/mL) or FBS (5%) for 48 hours and the lysates from these cells were subjected to Western blot analysis. As shown in Figure 16, bindarit significantly reduced the expression of SMemb in both TNF-α-stimulated cells (by 29% P<0.05 and 53% P<0.01, at 100 and 300 μM respectively) and FBS-stimulated cells (by 20% P<0.01 at 300 μM). The differentiated state of CASMCs induced by bindarit was also confirmed by the significant increased expression of α-SMA in both TNF-α-stimulated cells (by 87% P<0.05 and 132% P<0.01, at 100 and 300 μM respectively) and FBS-stimulated cells (by 69% P<0.01 at 300 μM). Treatment with bindarit at 300 μM also significantly increased calponin expression when compared with both TNF-α-stimulated cells by 172% (P<0.05) and FBS-stimulated cells by 100% (P<0.01).

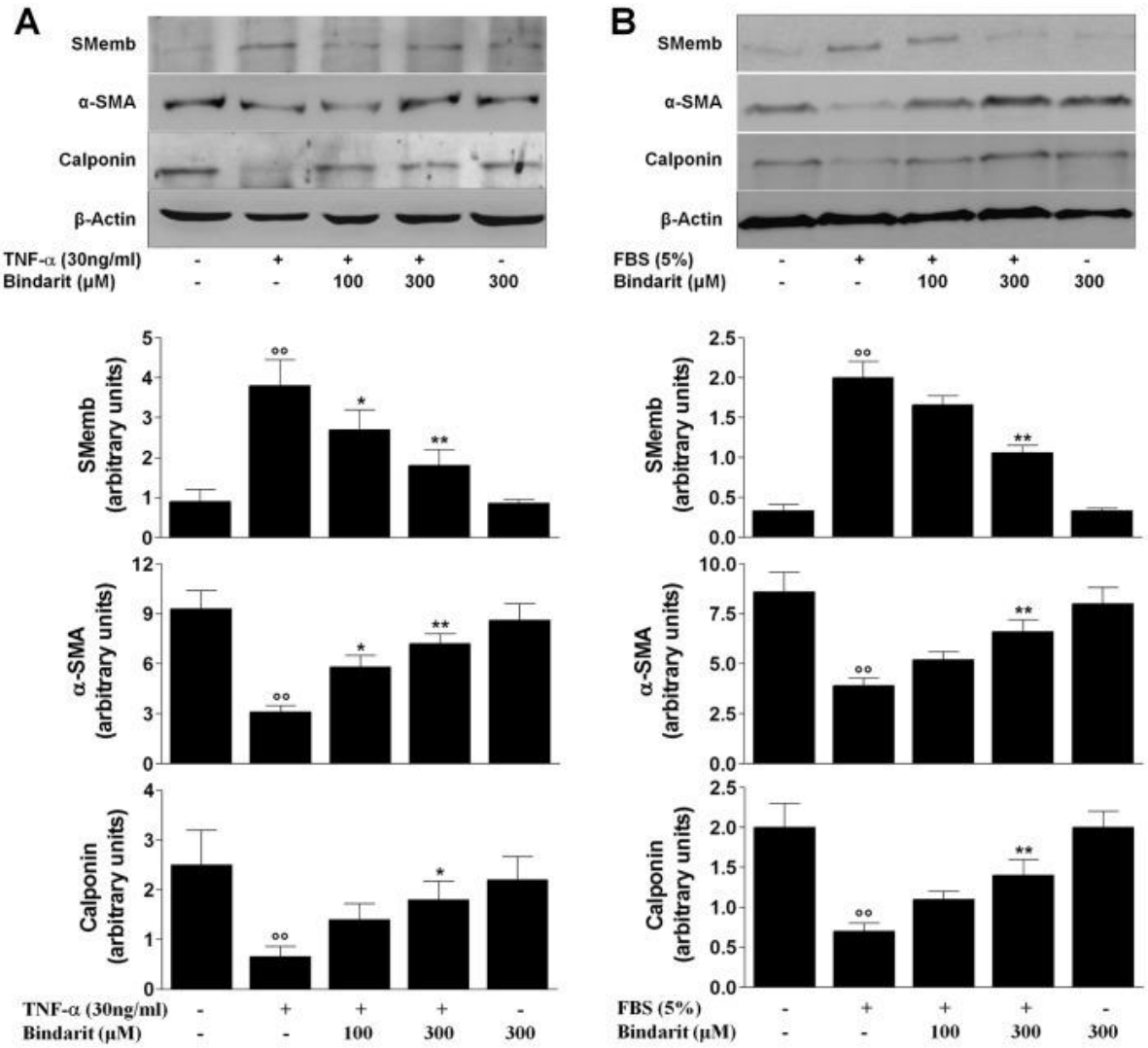

Figure 16
Effect of bindarit on contractile proteins expression in CASMCs. Representative Western blots and relative densitometric analysis showing the effects of bindarit (100 and 300 μM) on contractile proteins expression levels modulated by (A) TNF-α (30 ng/mL) or (B) FBS (5%). Results are expressed as mean±SEM of three separate experiments run in triplicate. °°P<0.01 *vs* unstimulated cells; *P<0.05, **P<0.01 *vs* untreated cells

3.3.2 CASMCs Morphological Changes induced by FBS

In addition to SMC-specific protein expression we examined SMC morphology. After 48 hours of stimulation with FBS (5%) the CASMCs were characterized by a flattened morphology as result of the dedifferentiation to a synthetic phenotype (Figure 17). Bindarit (300 μM) induced an elongated spindle-shaped phenotype, typical of a differentiated state (Figure 17).

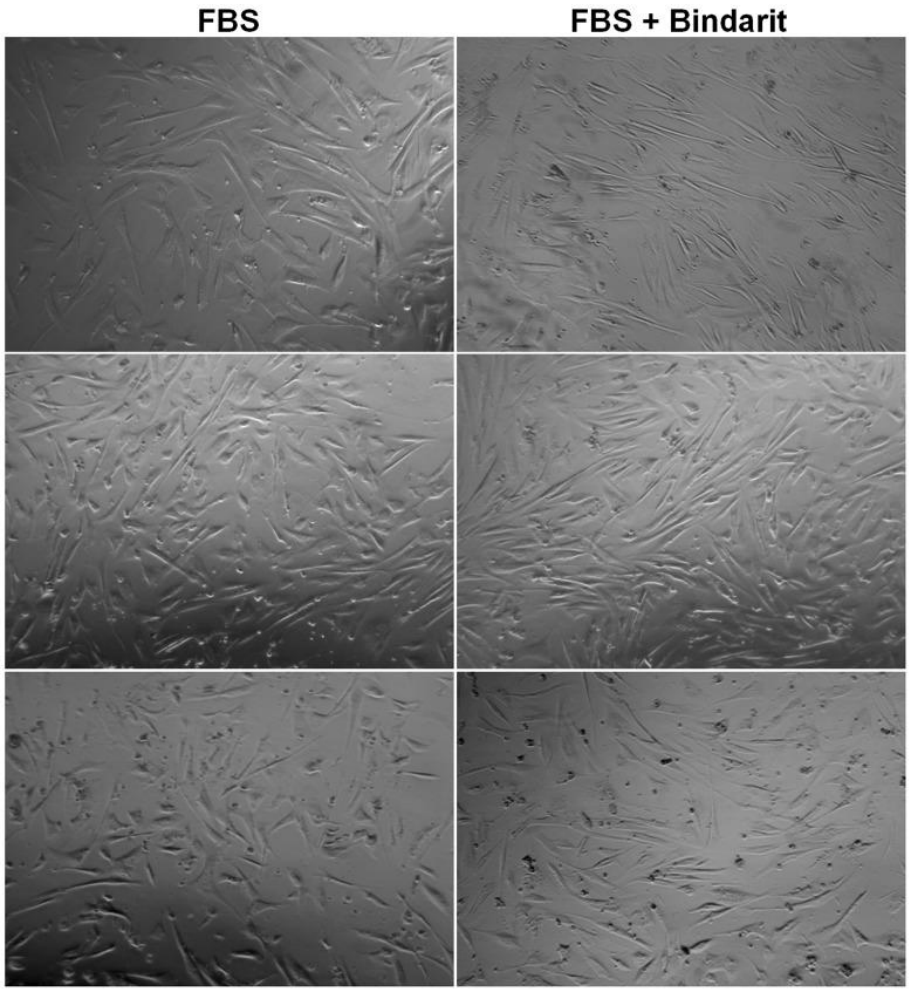

Figure 17
Effect of bindarit on morphological changes induced by FBS in CASMCs. Phase-contrast photomicrographs of CASMCs cultured in medium with 5% FBS for 48 hours with or without bindarit (300 μM)

3.3.3 CASMC Proliferation

SMCs plasticity exhibited in response to vascular injury, is characterized by both loss of VSMC-specific proteins expression and the increase in the proliferation. As shown in Figure 18A, bindarit at 10, 30, 100, and 300 μM significantly (P<0.01) inhibited TNF-α (30 ng/mL)-induced CASMC proliferation by 24%, 39%, 52% and 54%, respectively. Similar inhibitory effects of bindarit were observed in FBS (5%)- stimulated CASMCs (Figure 18A).

We also evaluated CASMC proliferation by directly counting the cells (Figure 18B). Bindarit, which was ineffective at 10 μM, significantly (P<0.01) inhibited the TNF-α-

induced CASMC number increase by 24%, 32% and 40%, at 30, 100, and 300 μM respectively. Similar inhibitory effects of bindarit were observed when FBS was used as stimulant (Figure 18B). Bindarit alone (300 μM) had no effect on cell proliferation/viability (Figure 18A and 18B).

3.3.4 CASMC Migration and Invasion

The higher proliferation rate of dedifferentiated SMCs is accompanied by increased mitogen-mediated migration. Therefore, we evaluated the effect of bindarit (10–300 μM) on TNF-α-induced VSMC chemotaxis. Bindarit significantly (P<0.01) inhibited chemotactic migration at 100 and 300 μM by 30% and 55%, respectively (Figure 18C). Moreover, bindarit (300 μM) significantly (P<0.01) reduced CASMC invasion by 50% through the Matrigel barrier which mimics extracellular matrix (Figure 18D). Bindarit alone (300 μM) had no effect on both migration and invasion (data not shown).

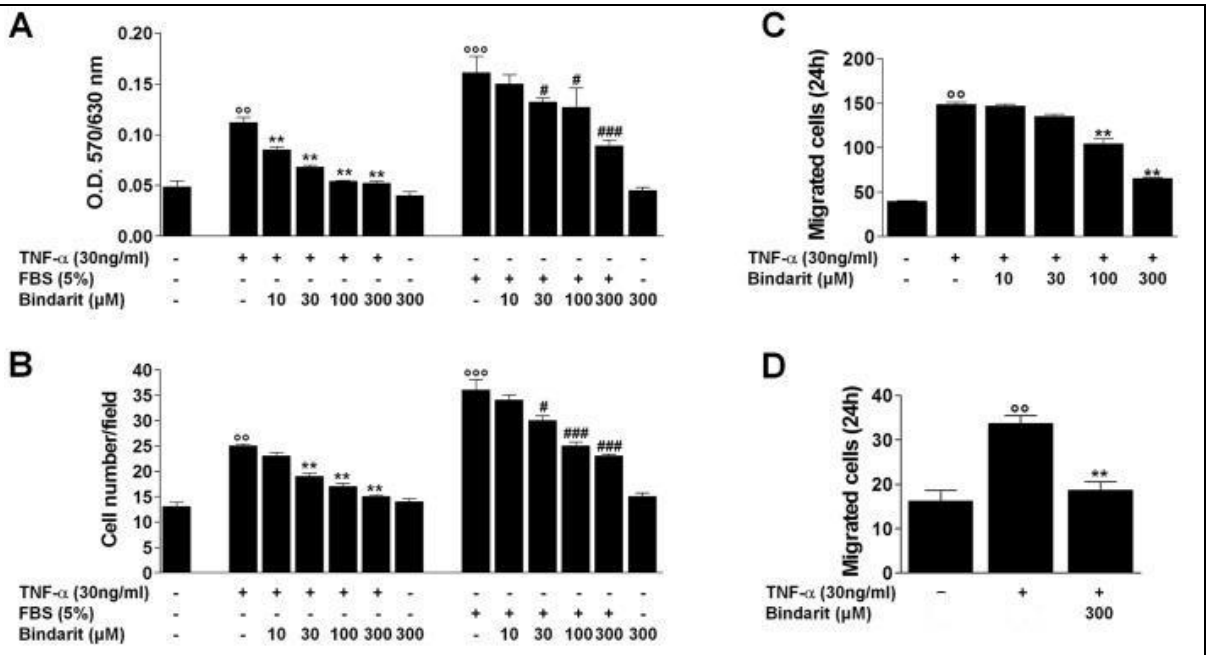

Figure 18
Effect of bindarit on CASMC proliferation, migration and invasion. CASMC proliferation assessed by MTT assay (**A**) and by cell counting expressed as number of cells per field (**B**). Effect of bindarit on CASMC migration (**C**) and invasion (**D**). Results are expressed as mean±SEM of three separate experiments run in triplicate. °°P<0.01, °°°P<0.001 *vs* unstimulated cells; **P<0.01 *vs* TNF-α-stimulated cells; $^{\#}P$<0.05, $^{\#\#\#}P$<0.001 *vs* FBS-stimulated cells.

3.3.5 MMP-2 and MMP-9 Activity in CASMCs

Subconfluent cultures of CASMCs were exposed to TNF-α (30 ng/mL) for 24 hours in the presence or absence of bindarit (300 μM) to assess gelatinase production. Gelatin zymography of control supernatants showed the constitutive release of the latent form of matrix metalloproteinase 2 (MMP-2), visualized as a bands at 72 kDa and 68 kDa. Neither the stimulation with TNF-α, nor the treatment with bindarit significantly modified the release of the active form (62 kDa) (Figure 19). The stimulation with TNF-α significantly (P<0.01) induced the release of MMP-9 (92 kDa) which was significantly (P<0.05) inhibited by bindarit (Figure 19).

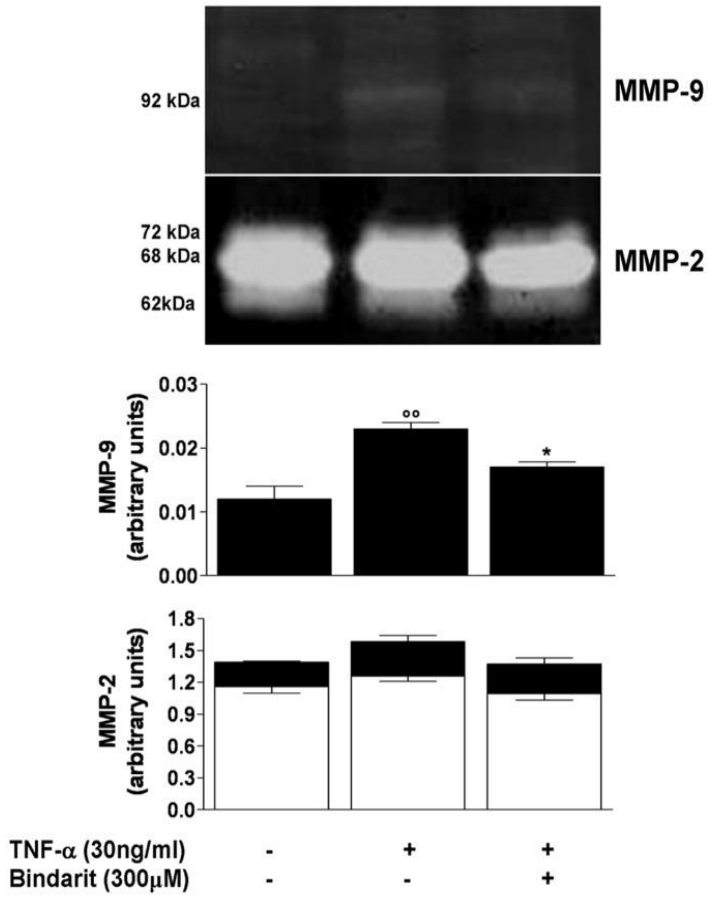

Figure 19
Effect of bindarit on MMP-2 and MMP-9 activity. Representative gel zymography of conditioned medium from TNF-α (30 ng/mL)-stimulated CASMCs and relative densitometric analysis showing the effect ofbindarit (300 μM) on MMP-9 activated form and both MMP-2 latent (white columns) and activated (black columns) forms. Results are expressed as mean±SEM of three experiments. °°P<0.01 *vs* unstimulated cells; °P<0.05 *vs* TNF-α-stimulated cells.

3.3.6 MCP-1 and MCP-3 Production in CASMCs

The effect of bindarit on MCP-1 and MCP-3 production by CASMCs was determined by ELISA. As shown in table 4, stimulation of CASMCs with TNF-α (30 ng/mL) or FBS (5%) caused a time-dependent increase of MCP-1 levels compared with unstimulated cells. Bindarit (10–300 μM) caused a significant concentration-related inhibition of MCP-1 production. As shown in table 5, bindarit (30-300 μM) significantly reduced MCP-3 production in TNF-α (30 ng/mL) stimulated CASMCs. FBS (5%) had no effect on MCP-3 production (data not shown). Bindarit alone (300 μM) did not significantly affect basal MCP-1 or MCP-3 levels (table 4 and 5).

	MCP-1 (ng/mL)		
	6 h	12 h	24 h
Unstimulated cells	0.1±0.01	0.4±0.04	2.1±0.02
Bindarit 300 μM	0.1±0.01	0.4±0.02	2.0±0.03
TNF-α 30 ng/ml	1.6±0.07°°	3.0±1.09°°	13.1±0.12°°
+ bindarit 10 μM	1.5±0.01	2.4±0.04**	11.5±0.15**
+ bindarit 30 μM	1.4±0.01*	2.1±0.02**	10.8±0.10**
+ bindarit 100 μM	1.3±0.02**	1.8±0.05**	10.3±0.29**
+ bindarit 300 μM	1.1±0.06**	1.5±0.05**	8.0±0.05**
FBS 5%	1.5±0.22	5.5±0.26^{+++}	23.5±1.89^{+++}
+ bindarit 10 μM	1.5±0.29	4.7±0.61	22.5±1.56
+ bindarit 30 μM	1.4±0.64	3.4±0.75	15.8±2.18$^{\#}$
+ bindarit 100 μM	1.3±0.74	2.6±0.55$^{\#\#}$	10.5±0.87$^{\#\#\#}$
+ bindarit 300 μM	1.0±0.34	2.5±0.30$^{\#\#}$	8.8±1.32$^{\#\#\#}$

Table 4
Effect of bindarit on MCP-1 production by TNF-α- or FBS-stimulated CASMCs. Results are expressed as mean ± SEM of three separate experiments run in triplicate. °°P<0.01, ^{+++}P<0.001*vs* unstimulated cells; *P<0.05, **P<0.01*vs* TNF-α-stimulated cells; $^{\#}P$<0.05, $^{\#\#}P$<0.01, $^{\#\#\#}P$<0.001 *vs* FBS-stimulated cells.

	MCP-3 (pg/mL)		
	6 h	12 h	24 h
Unstimulated cells	70.0±8.00	164.3±40.31	211.3±44.49
Bindarit 300 µM	90.3±9.40	178.3±53.35	210.3±52.61
TNF-α 30 ng/ml	116.9±25.71	501.0±78.48°°	714.3±87.83°°°
+ bindarit 10 µM	113.3±16.13	428.0±46.46	671.3±99.47
+ bindarit 30 µM	114.7±18.17	438.0±69.79	477.7±34.80
+ bindarit 100 µM	110.0±20.30	286.0±49.00	440.3±31.84
+ bindarit 300 µM	104.3±21.53	164.7±10.81*	151.3±6.36***

Table 5
Effect of bindarit on MCP-3 production by TNF-α-stimulated CASMCs. Results are expressed as mean±SEM of three separate experiments run in triplicate. °°P<0.01, °°°P<0.001 *vs* unstimulated cells; *P<0.05, **P<0.01, ***P<0.001 *vs* TNF-α-stimulated cells.

3.3.7 Contractile Proteins Expression in rat carotid arteries

As shown in Figure 20A, treatment with bindarit significantly reduced the expression of SMemb at 14 and 28 days (by 31%, P<0.001 and 37%, P<0.05, respectively) and increased the expression of calponin at 7 and 14 days (by 19%, P<0.05 and 47%, P<0.001). Bindarit also increased the expression of α-SMA at 14 and 28 days (by 13%, P<0.05 and 8%, P<0.01, respectively) and, as previously demonstrated, reduced the expression of PCNA at 7 days (by 44%, P<0.01) (Figure 20B).

Localization of contractile proteins in rat carotid arteries was performed by immunohistochemistry to determine the temporal expression and cellular localization. α-SMA resulted highly expressed in the medial SMCs of non-injured carotid sections (data not shown), while negative control IgG showed no signal (data not shown). At day 7, medial SMCs, close to the lumen, started to lose α-SMA staining, as consequence of changes in phenotype. At day 14, SMCs in the media and neointima, although stained with the anti-α-SMA antibody, showed weaker signal than the medial SMCs at day 7. At day 28, the α-SMA resulted highly expressed in the medial SMCs, instead the expression in the neointimal cells resulted still weak or absent. Although bindarit did not modify α-SMA localization, it determined a higher α-SMA expression in both media and neointima, at all time points considered (Figure 21A). Non-injured carotid sections lacked immunoreactive SMemb (data not shown). In contrast, injured carotid arteries showed a remarkable number of cells in the media and neointima strongly positive for SMemb, at all time points considered, while negative control IgG showed no signal (data not shown). The treatment with bindarit

reduced the number of the SMemb-positive cells at day 7 and, more interesting, the SMemb-positive cells resulted absent in the media at day 14 and 28 (Figure 21B). Immunoreactivity for calponin was visible in the medial SMCs of non-injured carotid sections (data not shown), while negative control IgG showed no signal (data not shown). At all time points considered, the injured arteries lacked immunoreactive calponin. Intriguingly, at day 7 and day 14, the vessels from bindarit-treated rats showed calponin signal in the medial SMCs (Figure 21C).

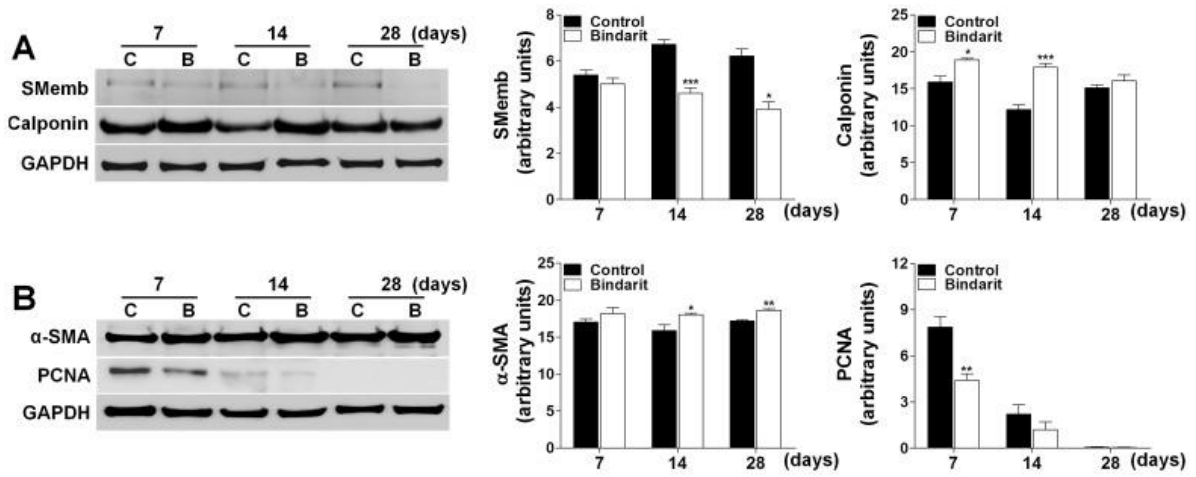

Figure 20
Effect of bindarit on contractile protein expression in rat carotid arteries. A and **B**. Representative Western blots and relative densitometric analysis showing the effect of the oral administration of bindarit (200 mg/Kg/day) on SMemb, calponin, α-SMA and PCNA expression levels in rat carotid arteries at days7, 14 and 28 days after injury. Results are expressed as mean ± SEM, where n = 4 pools. **P*<0.05, ***P*<0.01 and ****P*<0.001 *vs* control group.

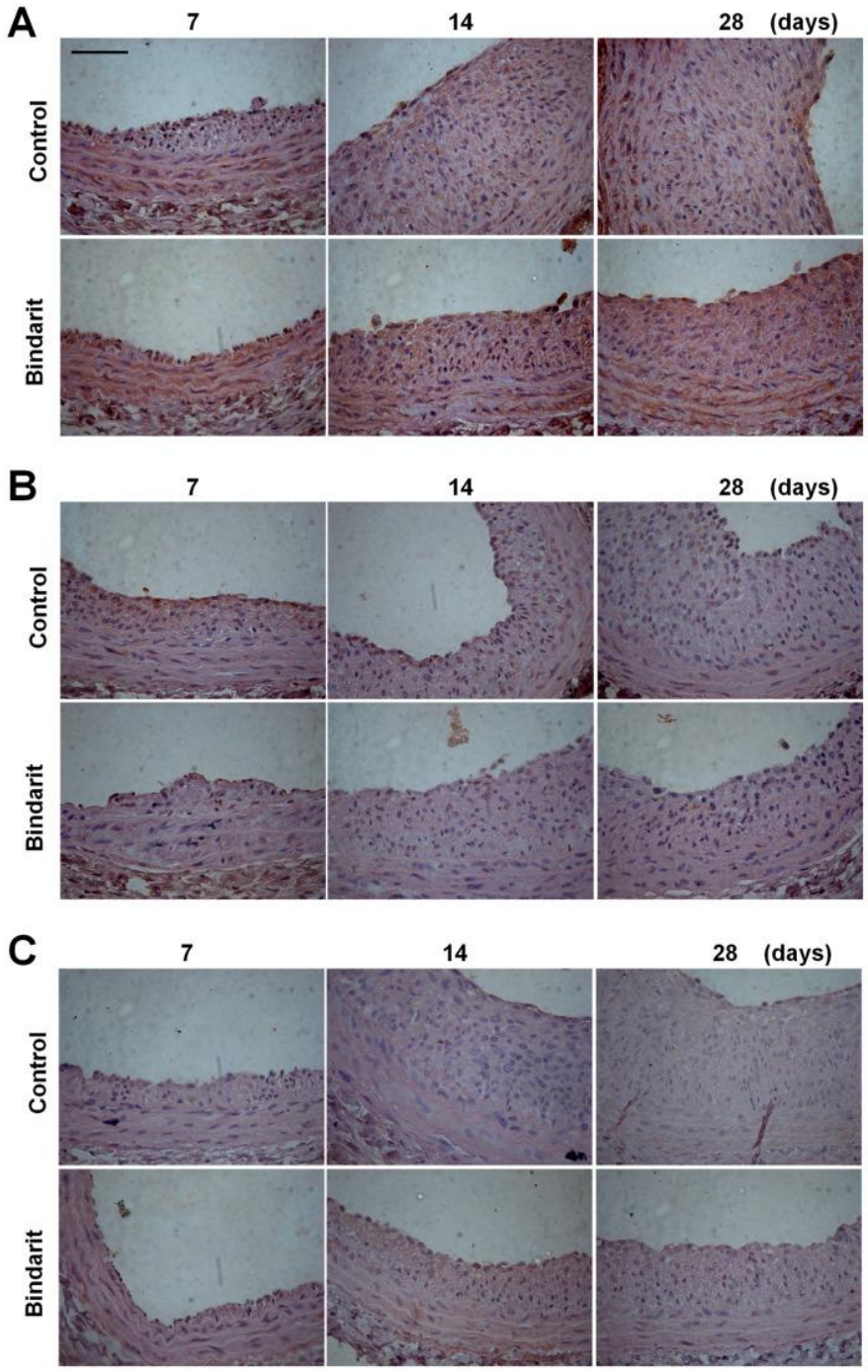

Figure 21
Effect of bindarit on contractile proteins localization in rat carotid arteries. Immohistochemical localization of α-SMA (**A**), SMemb (**B**) and calponin (**C**) expression in rat carotid arteries 7, 14 and 28 days after angioplasty. Bar = 100 μm.

4. DISCUSSION

The results provided in this thesis show that bindarit given systemically significantly reduced neointimal formation in animal models of arterial injury by inhibiting SMC proliferation/migration, and macrophage infiltration; these effects correlated with a reduction in MCP-1 synthesis.

Bindarit is an original compound selected by screening a series of indazolic derivatives endowed with peculiar anti-inflammatory activity associated with a selective inhibition of a subfamily of CC inflammatory chemokines, including MCP-1/CCL2, MCP-3/CCL7, and MCP-2/CCL8, showing no effect on other CC and CXC chemokines such as MIP-1a/ CCL3, MIP-1b/CCL4, MIP-3/CCL23, RANTES/CCL5, and IL8/ CXCL8 (Zoja C et al., 1998; Guglielmotti A et al., 2002; Bhatia M et al., 2005; Bhatia M et al., 2008; Mirolo M et al., 2008).

After vascular damage, the rat carotid artery develops neointimal formation, mainly due to proliferation and migration of SMCs, that causes a clear narrowing of the vessel lumen.

Neointima formation contributes to the development of restenosis after coronary artery angioplasty, with or without stenting, in which a pivotal mechanism is represented by the loss of differentiation of SMCs that were able to proliferate and migrate (Owens GK et al., 2004).

It is well known that among pro-inflammatory CC chemokines, MCP-1 is implicated in all these processes and the source of this chemokine is likely to include the major cells in injured arteries, such as endothelial cells, SMCs, and macrophages (Charo IF and Taubman MB, 2004).

In injured carotids arteries from rats treated with bindarit, a significant inhibition of neointima formation associated with a reduced MCP-1 production was observed. Bindarit did not modify MCP-1 localization but reduced MCP-1 expression in both media and neointima. Moreover, bindarit caused significant inhibition of MCP-1 serum levels. Increased levels of circulating MCP-1 in animals subjected to vascular injury are in keeping with an active role for this cytokine in tissue pathogenesis and correlate with epidemiological evidence showing higher MCP-1 plasma levels associated with human restenosis (Cipollone F et al., 2001; Martinovic I et al., 2005).

Bindarit showed in vivo anti-proliferative effects. Thus, bindarit diminished the number of PCNA-positive proliferating cells in the media and intima 7 days after rat balloon

angioplasty, concomitantly with the beginning of neointimal formation, without affecting re-endothelialization evaluated 14 days after injury.

It is well known that MCP-1 activity is in part due to recruitment of monocytes/macrophages that are responsible for local production of cytokines, but MCP-1 may also directly induce SMC proliferation and migration through cell cycle proteins and intracellular proliferative signals (Selzman CH et al., 2002; Massberg S et al., 2003; Parenti A et al., 2004).

Our results also showed that bindarit reduced monocytes/ macrophages recruitment in injured rat carotid arteries. The rat balloon angioplasty model could be considered ideal to study the proliferation of SMCs in vivo; however, it is not an ideal model for the study of monocytes/macrophages recruitment, considering the injury is performed in a non-atherosclerotic arterial bed (Reidy MA et al., 1992; Roque M et al., 2000).

It is well known that hypercholesterolaemia, a potent trigger of vessel wall inflammation in atherosclerosis, induces MCP-1 expression in SMCs and upregulates CCR2 in human monocytes, enhancing monocyte recruitment after arterial injury and thus mediates the exacerbation of neointimal growth (Yu X et al., 1992; Han KH et al., 1998; Oguchi S et al., 2000). In our experiments, no clear atherosclerotic lesions were detectable in the aortic root of mice 28 days after injury. However, we and others have demonstrated that lymphocytes already reside into the adventitia of arterial wall of apoE$^{-/-}$ mice even before the onset atherosclerosis (Galkina E et al., 2006; Maffia P et al., 2007). In this light, the hyperlipidaemic mice tool represents a step forward to the rat balloon angioplasty model, allowing us to study the effect of bindarit in the contest of increased vascular inflammation.

Our results clearly demonstrated that bindarit reduced neointima formation by reducing proliferating rate and macrophage infiltration, effects associated with a reduced expression of MCP-1 in injured vessels. In hypercholesterolaemic rabbits, gene transfer of a plasmid coding for a mutant form of MCP-1 appeared to reduce neointima formation after balloon injury, mainly inhibiting macrophage infiltration to the injured vessels (Mori E et al., 2002). Similarly, in hypercholesterolaemic apoE$^{-/-}$ mice also deficient in CCR2, neointimal lesions after wire injury of the carotid artery were diminished and showed a marked reduction in macrophage content compared with apoE$^{-/-}$/CCR2$^{+/+}$ mice (Schober A et al., 2004).

However, although small animal models of neointimal formation have several advantageous characteristics (eg, low cost, ready availability, small size that limits the quantities of investigational drugs required for in vivo use), on many occasions they lack

efficacy in predicting the success of interventions to inhibit restenosis in humans (Johnson GJ et al., 1999; Jeremy JY et al., 2010; Touchard AG et al., 2006). Therefore, we evaluated the efficacy of bindarit in the preclinical model of in stent stenosis in pigs.

Bindarit given orally significantly reduced in-stent stenosis in the porcine coronary stent model. When compared with the controls, stented arteries from bindarit-treated animals showed a significant reduction of morphometric percentage stenosis area, from 75% to 47.5%, a decrease of 37%. Seventy-five percent of the stenosis area in the control group was a higher value than other reports in the literature (Kasai T et al., 2008; Heldman AW et al., 2001). However, as shown by our injury score, no or minimal damage was induced to the media. According to the Gunn J (2002) scoring system, an average value of ≈2.2 indicates an IEL deformed >45° in most of the samples analyzed in the absence of medial injury. Injury scores, external elastic lamina area, IEL area, and stent circumference were similar in both groups, confirming the homogeneity of the analyzed data in our model. In stented coronary arteries from animals treated with bindarit, neointimal area was significantly inhibited by 40% compared with control animals. Importantly, bindarit shows effects similar to those of paclitaxel- and sirolimous-coated stents on neointima formation in porcine models (Suzuki T et al., 2001; Heldman AW et al., 2001). A moderate inflammation was also observed in peri-stent areas, as assessed by the inflammatory score, and this was reduced by ≈40% in stented arteries from bindarit-treated animals.

Neointimal hyperplasia contributes to the development of in-stent restenosis (Chieffo A et al., 2009), and a pivotal mechanism is the loss of differentiation of SMCs that become able to proliferate and migrate (Owens GK et al., 2004). Interestingly, bindarit diminished the number of arterial PCNA-positive proliferating cells 7 days after stent implantation and monocyte/macrophage content in injured vessels at 28 days, clearly showing either antiproliferative and antiinflammatory activity. These effects were associated with a significant inhibition of MCP-1 plasma levels. The present results have some limitations. Although the porcine coronary model seems to represent the human coronary artery response to stenting, mimicking several clinical conditions, including thrombosis and neointimal formation (Touchard AG et al., 2006), it does not precisely simulate human in-stent restenosis (Johnson GJ et al., Touchard AG et al., 2006). An important point in the present model is that stent implantation was performed in normal porcine coronary arteries, whereas in humans, much of the stent would be in contact with atheromatous plaque and not with media. Furthermore, in the present study the extent of in stent stenosis was examined

only at 28 days after stent implantation; for example, longer follow-up should be performed to assess the effect of bindarit on arterial healing.

Bindarit also displayed antiproliferative effects in vitro, with significant inhibition of SMC proliferation and migration, effects associated with a significant and concentration-related inhibition of MCP-1 amounts measured in the supernatants of stimulated cells treated with bindarit. In the arterial wall, SMCs normally exist in a quiescent, differentiated state, representing the contractile phenotype. During neointimal formation SMCs became activated and change towards the synthetic phenotype characterised by a high rate of proliferation and chemotactic response, changes in the cytoskeleton composition (Owens GK et al., 2004) and increased expression of extracellular matrix proteins, cytokines and chemokines (Owens GK et al., 2004; Charey DJ et al., 1991; Schober A, 2008).

It is well known that chemokines mediate SMC activation during vascular injury (Schober A, 2008; Schober A et al., 2004), with MCP-1 (Selzman CH et al., 2002) and MCP-3 (Maddaluno M et al., 2012) shown to directly induce human SMC proliferation and MCP- 1 shown to induce cell migration (Parenti A et al., 2004) and the functional switch from the contractile to the synthetic phenotype (Denger S et al., 1999). This process is characterized by the downregulation of the differentiation markers such as α-SMA and calponin, concurrent with the upregulation of SMemb, that typifies immature SMCs (Owens GK et al., 2004). Importantly, it is now well established that differentiation and proliferation are not mutually exclusive and that many factors other than SMC proliferation status influence the differentiation state. Inhibition of proliferation alone is not sufficient to promote SMC differentiation (Alexander MR and Owens GK, 2012). However, anti proliferative agents used for inhibition of experimental neointimal formation, like simvastatin (Indolfi C et al., 2000), or human restenosis, like rapamycin (Martin KA et al. 2007), are also able to induce SMC differentiated phenotype (Martin KA et al. 2007; Wada H et al., 2008). As above reported, bindarit is a selective inhibitor of MCP-1/CCL2, MCP-3/CCL7, and MCP-2/CCL8 synthesis (Mirolo M et al., 2008) acting through the down-regulation of NF-kB pathway (Mora E et al., 2012). To better understand the effect of bindarit on human SMC, we evaluated the phenotypic modulation of CASMC analyzing the contractile proteins (α-SMA, calponin and SMemb) expression. α-SMA is known to be expressed in a wide variety of non-vascular SMC cell types, under certain circumstances, for this reason we also analyzed calponin, that is univocally expressed by fully differentiated, mature SMC (Owens GK, 2004). We observed that the expression of contractile proteins in CASMCs changed in response to stimulation with FBS and the proinflammatory cytokine

TNF-α, with a reduction of α-SMA and calponin, and a concomitant increase of SMemb. These changes were significantly reversed by bindarit. CASMCs grown in presence of FBS exhibited a flattened morphology, feature of the synthetic phenotype. After bindarit treatment cells acquired the elongated and spindle-shaped morphology, typical feature of the contractile phenotype. Further bindarit inhibited CASMC proliferation, migration and invasion through the Matrigel barrier and reduced metalloproteinase (MMP)-9 activity, which is known to be key for VSMC migration into the intimal area (Newby AC et al., 2000; Bendeck MP et al., 1994). Bindarit also reduced the levels of both MCP-1 and MCP-3, data in line with results observed both in aortic rat and mice SMCs, as well as in pig coronary SMCs.

The effect of bindarit on SMC phenotypic switching was confirmed in vivo in the rat carotid arteries subjected to balloon-induced endothelial denudation, an ideal experimental model for studying VSMC behavior (Selzman CH et al., 2002). The inhibition of neointimal formation observed in bindarit treated rats was associated with a modulation of the contractile proteins expression patterns. Indeed, treatment with bindarit reduced the expression of SMemb and increased the expression of α-SMA and calponin after vascular injury. These results demonstrates that bindarit regulates the contractile proteins expression and phenotype switching of SMCs, suggesting a novel underlying mechanisms by which bindarit can inhibit neointimal formation in human restenosis.

5. CONCLUSION

The exploitation of the chemokine system as a drug target in vascular pathology has relied mainly on the development of receptor antagonists and blocking antibodies (Charo IF and Taubman MB, 2004). However, the attempt to block chemokines and their receptors in humans is more complex (Mirolo M et al., 2008).

Here, we report the use of oral administration of bindarit as a viable approach to reduce neointimal hyperplasia in stent stenosis in pigs. Preclinical studies demonstrated that bindarit has a safe toxicological profile (rodent LD50 ≈2000 mg/kg PO and ≈600 mg/kg IP) and is devoid of immunosuppressive, mutagenic, and carcinogenic effects (Product Data Sheet, Angelini Research Center). Phase I clinical studies demonstrated that bindarit (up to a dose of 1200 mg BID) is well tolerated and confirmed the lack of overt toxicity suggested by preclinical studies (Product Data Sheet, Angelini Research Center). Results of Phase II clinical studies confirmed the good tolerability profile of bindarit and demonstrated, at 600 mg BID, significant effects in kidney disease patients (Guglielmotti A et al., 2009; Ruggenenti P, 2009).

Importantly, a double-blind, randomized, placebo-controlled phase II clinical trial ("The Effects of Bindarit in Preventing Stent Restenosis", registered on ClinicaTrisl.gov, NCT 01269242), with the aim of investigating the effect of bindarit in human coronary restenosis, showed that bindarit induced a significant reduction of in-stent late loss (Colombo A et al., 2012).

In conclusion, evidence of bindarit efficacy could provide clinicians with useful complementary or alternative therapeutic tools.

6. REFERENCES

1. Alexander MR, Owens GK. Epigenetic control of smooth muscle cell differentiation and phenotypic switching in vascular development and disease. Annu Rev Physiol. 2012; 74: 13–40.

2. Apostolakis S, Papadakis EG, Krambovitis E, Spandidos DA. Chemokines in vascular pathology (review). Int J Mol Med. 2006;17(5):691-701

3. Asahara T, Chen D, Tsurumi Y, Kearney M, Rossow S, Passeri J, et al. Accelerated restitution of endothelial integrity and endothelium-dependent function after phVEGF$_{165}$ gene transfer. Circulation. 1996;94:3291–3302.

4. Bauters C, de Groote P, Adamantidis M, Delcayre C, Hamon M, Lablanche JM, Bertrand ME, Dupuis B, Swynghedauw B. Proto-oncogene expression in rabbit aorta after wall injury. First marker of the cellular process leading to restenosis after angioplasty? Eur Heart J. 1992;13(4):556-9.

5. Bendeck MP, Zempo N, Clowes AW, Galardy RE, Reidy MA. Smooth muscle cell migration and matrix metalloproteinase expression after arterial injury in the rat. Circ Res. 1994; 75: 539–545.

6. Bhatia M, Devi Ramnath RD, Chevali L, Guglielmotti A. Treatment with bindarit, a blocker of MCP-1 synthesis, protects mice against acute pancreatitis. Am J Physiol Gastrointest Liver Physiol. 2005;288:G1259–G1265.

7. Bhatia M, Landolfi C, Basta F, Bovi G, Ramnath RD, de Joannon AC, Guglielmotti A. Treatment with bindarit, an inhibitor of MCP-1 synthesis, protects mice against trinitrobenzene sulfonic acid-induced colitis. Inflamm Res. 2008;57:464–471.

8. Boring L, Gosling J, Cleary M et al. Decreased lesion formation in CCR2−/− mice reveals a role for chemokines in the initiation of atherosclerosis. Nature 1998;394:894–7

9. Chandrasekar B, Tanguay JF. Platelets and restenosis. J Am Coll Cardiol. 2000; 35: 555-562.

10. Charey DJ. Control of growth and differentiation of vascular cells by extracellular matrix proteins. Annu Rev Physiol. 1991; 53: 161–177. [PubMed]

11. Charo IF, Taubman MB. Chemokines in the pathogenesis of vascular disease. Circ Res. 2004;95:858–866.

12. Chieffo A, Foglieni C, Nodari RL, Briguori C, Sangiorgi G, Latib A, Montorfano M, Airoldi F, Michev I, Carlino M, Colombo A, Maseri A. Histopathology of clinical coronary restenosis in drug-eluting versus bare metal stents. Am J Cardiol. 2009;104:1660 –1667.

13. Cipollone F, Marini M, Fazia M, Pini B, Iezzi A, Reale M, Paloscia L, Materazzo G, D'Annunzio E, Conti P, Chiarelli F, Cuccurullo F, Mezzetti A. Elevated circulating levels of monocyte chemoattractant protein-1 in patients with restenosis after coronary angioplasty. Arterioscler Thromb Vasc Biol. 2001;21:327–334.

14. Colombo A, Limbruno U, Lettieri C, Lioy E, Guglielmotti A, et al. A double blind randomized study to evaluate the efficacy of bindarit in preventing coronary stent restenosis. J Am Coll Cardiol. 2012; 59: E11–E11.

15. Costa MA, Simon DI. Molecular basis of restenosis and drug-eluting stents. Circulation. 2005; 111: 2257-2273.

16. Denger S, Jahn L, Wende P, Watson L, Gerber SH, et al. Expression of monocyte chemoattractant protein-1 cDNA in vascular smooth muscle cells: induction of the synthetic phenotype: a possible clue to VSMC differentiation in the process of atherogenesis. Atherosclerosis. 1999; 144: 15–23.

17. Dimayuga PC, Chyu KJ and Cercek B. Immune responses regulating the response to vascular injury. Current Opinion in Lipidology 2010;21:416–421.

18. Dimayuga PC, Li H, Chyu KJ. T cell modulation of intimal thickening after vascular injury: the bimodal role of IFN-gamma in immune deficiency. Arterioscler Thromb Vasc Biol. 2005;25:2528-2534.

19. Egashira K, Koyanagi M, Kitamoto S, Ni W, Kataoka C, Morishita R, Kaneda Y, Akiyama C, Nishida KI, Sueishi K, Takeshita A. Antimonocyte chemoattractant protein-1 gene therapy inhibits vascular remodeling in rats: blockade of MCP-1 activity after intramuscular transfer of a mutant gene inhibits vascular remodeling induced by chronic blockade of NO synthesis. FASEB J. 2000;14:1974 –1978.

20. Egashira K, Nakano K, Ohtani K, Funakoshi K, Zhao G, Ihara Y, Koga J, Kimura S, Tominaga R, Sunagawa K. Local delivery of anti-monocyte chemoattractant protein-1 by gene-eluting stents attenuates in-stent stenosis in rabbits and monkeys. Arterioscler Thromb Vasc Biol. 2007;27: 2563–2568.

21. Egashira K, Zhao Q, Kataoka C et al. Importance of monocyte chemoattractant protein-1 pathway in neointimal hyperplasia after periarterial injury in mice. CircRes 2002;90:1167–2.

22. Furukawa Y, Matsumori A, Ohashi N, Shioi T, Ono K, Harada A, Matsushima K, Sasayama S. Anti-monocyte chemoattractant protein-1/monocyte chemotactic and activating factor antibody inhibits neointimal hyperplasia in injured rat carotid arteries. Circ Res. 1999;84:306 –314.

23. Galis ZS and Khatri JJ. Matrix metalloproteinases in vascular remodelling and atherogenesis: the good, the bad and the ugly. Circ Res. 2002; 90, 251-262.

24. Galis ZS, Sukhova GK, Lark MW et al. Increased expression of matrix metalloproteinases and matrix degrading activity in vulnerable regions of human atherosclerotic plaques. J Clin Invest. 1994;94:2493-503.

25. Galkina E, Kadl A, Sanders J, Varughese D, Sarembock IJ, Ley K. Lynphocyte recruitment into the aortic wall before and during development of atherosclerosis is partially L-selectin dependent. J Exp Med. 2006;203:1273–1282.

26. Guglielmotti A, D' Onofrio E, Coletta I, Aquilini L, Milanese C, Pinza M. Amelioration of rat adjuvant arthritis by therapeutic treatment with bindarit, an inhibitor of MCP-1 and TNF-α production. Inflamm Res. 2002;51:252–258.

27. Guglielmotti A, Orticelli G, Di Loreto G, Paolo D. Bindarit decreases monocyte chemoattractant protein-1 urinary excretion in humans: a pilot study in active lupus nephritis patients. Inflammation Res. 2009;58:S169.

28. Gunn J, Arnold N, Chan KH, Shepherd L, Cumberland DC, Crossman DC. Coronary artery stretch versus deep injury in the development of in-stent neointima. Heart. 2002;88:401– 405.

29. Han JW, Shimada K, Ma-Krupa W et al. Vessel wall-embedded dendritic cells induce T-cell autoreactivity and initiate vascular inflammation. Circ Res. 2008;102:546-553.

30. Han KH, Tangirala RK, Green SR, Quehenberger O. Chemokine receptor CCR2 expression and monocyte chemoattractant protein-1-mediated chemotaxis in human monocytes. Arterioscl Thromb Vasc Biol. 1998;18:1983–1991.

31. Hansson GK, Holm J, Holm S et al. T lymphocytes inhibit the vascular response to injury. Proc Natl Acad Sci U S A. 1991;88:10530-4.

32. Hayden MS and Ghosh S. Shared principles in NF-kappaB signaling. Cell. 2008;132:344-62.

33. Heldman AW, Cheng L, Jenkins GM, Heller PF, Kim DW, Ware M Jr, Nater C, Hruban RH, Rezai B, Abella BS, Bunge KE, Kinsella JL, Sollott SJ, Lakatta EG, Brinker JA, Hunter WL, Froehlich JP. Paclitaxel stent coating inhibits neointimal hyperplasia at 4 weeks in a porcine model of coronary restenosis Circulation. 2001;103:2289 –2295.

34. Ialenti A, Grassia G, Gordon P, Maddaluno M, Di Lauro MV, et al. Inhibition of in-stent stenosis by oral administration of bindarit in porcine coronary arteries. Arterioscler Thromb Vasc Biol. 2011; 31: 2448–54.

35. Indolfi C, Cioppa A, Stabile E, Di Lorenzo E, Esposito G, et al. Effects of hydroxymethylglutaryl coenzyme a reductase inhibitor simvastatin on smooth muscle cell proliferation in vitro and neointimal formation in vivo after vascular injury. J Am Coll Cardiol. 2000; 35: 214–21.

36. Indolfi C, Coppola C, Torella D et al. Gene therapy for restenosis after balloon angioplasty and stenting. Cardiol Rev. 1999;7: 324-331.

37. Jeremy JY, Thomas AC. Animal models for studying neointima formation. Curr Vasc Pharmacol. 2010;8:198 –219. 20.

38. Johnson GJ, Griggs TR, Badimon L. The utility of animal models in the preclinical study of interventions to prevent human coronary artery restenosis: analysis and recommendations. On behalf of the Subcommittee on Animal, Cellular and Molecular Models of Thromb Haemost of the Scientific and Standardization Committee of the International Society on Thromb Haemost. Thromb Haemost. 1999;81:835– 843.

39. Karin M. Nuclear factor-kappaB in cancer development and progression. Nature. 2006; 441: 431-6.

40. Kasai T, Miyauchi K, Yokoyama T, Kajimoto K, Sumiyoshi K, Kubota N, Ikeda E, Daida H. Pioglitazone attenuates neointimal thickening via suppression of the early inflammatory response in a porcine coronary after stenting. Atherosclerosis. 2008;197:612– 619.

41. Kodali RB, Kim WJ, Galaria II et al. CCL11 (Eotaxin) induces CCR3-dependent smooth muscle cell migration. Arterioscler Thromb Vasc Biol. 2004;24:1211-1216.

42. Kornowski R, Hong MK, Tio FO, Bramwell O, Wu H, Leon MB. In-stent restenosis: contributions of inflammatory responses and arterial injury to neointimal hyperplasia. J Am Coll Cardiol. 1998;31:224 –230.

43. Lagerqvist B, James SK, Stenestrand U, Lindbäck J, Nilsson T, Wallentin L. SCAAR Study Group. Long-term outcomes with drug-eluting stents versus bare-metal stents in Sweden. N Engl J Med. 2007; 356:1009-19.

44. Lin J, Zhu X, Chade AR, Jordan KL, Lavi R, Daghini E, Gibson ME, Guglielmotti A, Lerman A, Lerman LO. Monocyte chemoattractant proteins mediate myocardial microvascular dysfunction in swine renovascular hypertension. Arterioscler Thromb Vasc Biol. 2009;29:1810–1816.

45. Lincoff AM, Topol EJ, Ellis SG. Local drug delivery for the prevention of restenosis. Fact, fancy, and future. Circulation. 1994; 90: 2070-2084.

46. Maddaluno M, DiLauro MV, Di Pascale A, Santamaria R, Guglielmotti A, et al. Monocyte chemotactic protein-3 induces human coronary smooth muscle cell proliferation. Atherosclerosis. 2011; 217: 113–9.

47. Maffia P, Grassia G, Di Meglio P, Carnuccio R, Berrino L, Garside P, et al. Neutralization of interleukin-18 inhibits neointimal formation in a rat model of vascular injury. Circulation. 2006;114:430–437.

48. Maffia P, Zinselmeyer BH, Ialenti A, Kennedy S, Baker A, McInnes IB, et al. Multiphoton microscopy for 3-dimensional imaging of lymphocyte recruitment into apolipoprotein-E-deficient mouse carotid artery. Circulation. 2007;115:e326–e328.

49. Martin KA, Merenick BL, Ding M, Fetalvero KM, Rzucidlo EM, et al. Rapamycin promotes vascular smooth muscle cell differentiation through insulin receptor substrate-1/phosphatidylinositol 3-kinase/akt2 feedback signaling. J Biol Chem. 2007; 282: 36112–36120.

50. Martinovic I, Abegunewardene N, Seul M, Vosseler M, Horstick G, Buerke M, et al. Elevated monocyte chemoattractant protein-1 serum levels in patients at risk for coronary artery disease. Circ J. 2005;69:1484–1489.

51. Massberg S, Vogt F, Dickfeld T, Brand K, Page S, Gawaz M. Activated platelets trigger an inflammatory response and enhance migration of aortic smooth muscle cells. Thromb Res. 2003;110:187–194.

52. Mirolo M, Fabbri M, Sironi M, Vecchi A, Guglielmotti A, Mangano G, Biondi G, Locati M, Mantovani A. Impact of the anti-inflammatory agent bindarit on the chemokinome: selective inhibition of the monocyte chemotactic proteins. Eur Cytokine Netw. 2008;19:119–122.

53. Mitra AK and Agrawal DK. In stent restenosis: bane of the stent era. J. Clin. Pathol. 2006; 59; 232-239.

54. Mora E, Guglielmotti A, Biondi G, Sassone-Corsi P. Bindarit: an anti-inflammatory small molecule that modulates the NFκB pathway. Cell Cycle. 2012; 11: 159–69.

55. Mori E, Komori K, Yamaoka T, Tanii M, Kataoka C, Takeshita A, et al. Essential role of monocyte chemoattractant protein-1 in development of restenotic changes (neointimal hyperplasia and constrictive remodeling) after balloon angioplasty in hypercholesterolemic rabbits. Circulation. 2002;105:2905–2910.

56. Nakano K, Egashira K, Ohtani K, Zhao G, Funakoshi K, Ihara Y, Sunagawa K. Catheter-based adenovirus-mediated anti-monocyte chemoattractant gene therapy attenuates in-stent neointima formation in cynomolgus monkeys. Atherosclerosis. 2007;194:309 – 316.

57. Newby AC, Zaltsman AB. Molecular mechanisms in intimal hyperplasia. J Pathol. 2000; 190: 300–309.

58. Oguchi S, Dimayuga P, Zhu J, Chyu KY, Yano J, Shah PK, et al. Monoclonal antibody against vascular cell adhesion molecule-1 inhibits neointimal formation after periadventitial carotid artery injury in genetically hypercholesterolemic mice. Arterioscl Thromb Vasc Biol. 2000;20:1729–1736.

59. Owens GK, Kumar MS, Wamhoff BR. Molecular regulation of vascular smooth muscle cell differentiation in development and disease. Physiol Rev. 2004;84:767–801.

60. Parenti A, Bellik L, Brogelli L, Filippi S, Ledda F. Endogenous VEGF-A is responsible for mitogenic effects of MCP-1 on vascular smooth muscle cells. Am J Physiol Heart Circ Physiol. 2004;286:H1978–H1984.

61. Perico N, Benigni A, Remuzzi G. Present and future drug treatments for chronic kidney diseases: evolving targets in renoprotection. Nat Rev Drug Discov. 2008;7:936–853.

62. Peters S, Götting B, Trümmel M, Rust H, Brattström A. Valsartan for prevention of restenosis after stenting of type B2/C lesions: the VAL-PREST trial. J Invasive Cardiol. 2001; 13: 93-7.

63. Rao GN and Berk BC. Active oxygen species stimulate vascular smooth muscle cell growth and pro-oncogene expression. Circ Res. 1992; 70: 593-599.

64. Reidy MA, Fingerle J, Lindner V. Factors controlling the development of arterial lesions after injury. Circulation. 1992;86:III-43–III-46.

65. Remskar M, Li H, Chyu KY et al. Absence of CD40 signaling is associated with an increase in intimal thickening after arterial injury. Circ Res. 2001;88:390-4.

66. Roque M, Fallon JT, Badimon JJ, Zhang WX, Taubman MB, Reis ED. Mouse model of femoral artery denudation injury associated with the rapid accumulation of adhesion molecules on the luminal surface and recruitment of neutrophils. Arterioscler Thromb Vasc Biol. 2000;20:335–342.

67. Rostène W, Kitabgi P and Parsadaniantz SM. Chemokines: a new class of neuromodulator? Nat Rev Neurosci. 2007;8:895-903. Review.

68. Ruggenenti P. Effects of MCP-1 inhibition by bindarit therapy in type 2 diabetes subjects with micro- or macro-albuminuria. J Am Soc Nephrol. 2009;21:44A.

69. Schober A, Zernecke A, Liehn EA, von Hundelshausen P, Knarren S, Kuziel WA, et al. Crucial role of the CCL2/CCR2 axis in neointimal hyperplasia after arterial injury in hyperlipidemic mice involves early monocyte recruitment and CCL2 presentation on platelets. Circ Res. 2004; 95:1125–1133.

70. Schober A. Chemokines in vascular dysfunction and remodeling. Arterioscler Thromb Vasc Biol. 2008;28:1950–1959.

71. Selzman CH, Miller SA, Zimmerman MA, Gamboni-Robertson F, Harken AH, Banerjee A. Monocyte chemotactic protein-1 directly induces human vascular smooth muscle proliferation. Am J Physiol Heart Circ Physiol. 2002;283:H1455–H1461.

72. Serruys PW, Luijten HE, Beatt KJ, Geuskens R, de Feyter PJ, van den Brand M, Reiber JH, ten Katen HJ, van Es GA and Hugenholtz PG. Incidence of restenosis after successful coronary artery angioplasty: a time-related phenomenon. A quantitative angiographic study in 342 consecutive patients at 1,2,3 and 4 months. Circulation. 1988; 77: 361-371.

73. Sherr CJ, Roberts JM. CDK inhibitors: Positive and negative regulators of G1-phase progression. Genes & Dev. 1999; 13: 1501-1512.

74. Suzuki T, Kopia G, Hayashi S, Bailey LR, Llanos G, Wilensky R, Klugherz BD, Papandreou G, Narayan P, Leon MB, Yeung AC, Tio F, Tsao PS, Falotico R, Carter AJ. Stent-based delivery of sirolimus reduces neointimal formation in a porcine coronary model. Circulation. 2001; 104:1188 –1193.

75. Takagi T, Akasaka T, Yamamuro A, Honda Y, Hozumi T, Morioka S, Yoshida K. Troglitazone reduces neointimal tissue proliferation after coronary stent implantation in patients with noninsulin dependent diabetes

mellitus: a serial intravascular ultrasound study. J Am Coll Cardiol 2000; 36: 1529–35.

76. Tanabe Y, Ito E, Nakagawa I, Suzuki K. Effect of cilostazol on restenosis after coronary angioplasty and stenting in comparison to conventional coronary artery stenting with ticlopidine. Int J Cardiol 2001; 78: 285-91.

77. Tardif JC, Cote G, Lesperance J, Bourassa M, Lambert J, Doucet S, Bilodeau L, Nattel S and de GP. Probucol and multivitamins in the prevention of restenosis after coronary angioplasty. Multivitamins and Probucol Study Group. N Engl J Med. 1997; 337: 365-372.

78. Topol EJ, Serruys PW. Frontiers in interventional cardiology. Circulation. 1998; 98: 1802-1820.

79. Touchard AG, Schwartz RS. Preclinical restenosis models: challenges and successes. Toxicol Pathol. 2006;34:11–18.

80. Toutouzas K, Colombo A and Stefanadis C. Inflammation and restenosis after percutaneous coronary interventions. Eur Heart J. 2004;25:1679-87.

81. Virmani R, Farb A and Burke AP. Coronary angioplasty from the perspective of the atherosclerotic plaque: Morphologic predictors of immediate success and restenosis. Am Heart J. 1994; 127: 163- 179.

82. Wada H, Abe M, Ono K, Morimoto T, Kawamura T, et al. Statins activate GATA-6 and induce differentiated vascular smooth muscle cells. Biochem Biophys Res Commun. 2008; 374: 731–736.

83. Walter DH, Schächinger V, Elsner M, Mach S, Auch-Schwelk W, Zeiher AM. Effect of statin therapy on restenosis after coronary stent implantation. Am J Cardiol. 2000; 85: 962-8.

84. Welt FGP and Rogers C. Inflammation and restenosis in the stent era. Arterioscler Thromb Vasc Biol. 2002;22:1769-76.

85. Whan Lee C, Kim SH, Suh J, Park DW, Lee SH, Kim YH, Hong MK, Kim JJ, Park SW, Park SJ. Long-term clinical outcomes after sirolimus-eluting stent implantation for treatment of restenosis within bare-metal versus drug-eluting stents. Catheter Cardiovasc Interv. 2008; 71: 594-8.

86. Work LM, McPhaden AR, Pyne NJ, Pyne S, Wadsworth RM, Wainwright CL. Short-term local delivery of an inhibitor of Ras farnesyltransferase prevents neointima formation in vivo after porcine coronary balloon angioplasty. Circulation. 2001;104:1538 –1543.

87. Yan BP, Duffy SJ, Clark DJ, Lefkovits J, Warren R, Gurvitch R, Lew R, Sebastian M, Brennan A, Andrianopoulos N, Reid CM, Ajani AE; Melbourne Interventional Group. Rates of Stent Thrombosis in Bare-Metal Versus Drug-Eluting Stents (from a Large Australian Multicenter Registry). Am J Cardiol. 2008; 101: 1716-22.

88. Yoshida T and Owens GK. Molecular determinants of vascular smooth muscle cell diversity. Circ Res. 2005;96:280-291.

89. Yu X, Dluz S, Graves DT, Zhang L, Antoniades HN, Hollander W, et al. Elevated expression of monocyte chemoattractant protein 1 by vascular smooth muscle cells in hypercholesterolemic primates. Proc Natl Acad Sci USA. 1992;89:6953–6957.

90. Yue TL, Vickery-Clark L, Louden CS, Gu JL, Ma XL, Narayanan PK, et al. Selective estrogen receptor modulator idoxifene inhibits smooth muscle cell proliferation, enhances reendothelialization, and inhibits neointimal formation in vivo after vascular injury. Circulation. 2000;102:III281–III288.

91. Zhu XY, Chade AR, Krier JD, Daghini E, Lavi R, Guglielmotti A, Lerman A, Lerman LO. The chemokine monocyte chemoattractant protein-1 contributes to renal dysfunction in swine renovascular hypertension. J Hypertens. 2009;27:2063–2073.

92. Zoja C, Corna D, Benedetti G, Morigi M, Donadelli R, Guglielmotti A, Pinza M, Bertani T, Remuzzi G. Bindarit retards renal disease and prolongs survival in murine lupus autoimmune disease. Kidney Int. 1998; 53:726 –734.